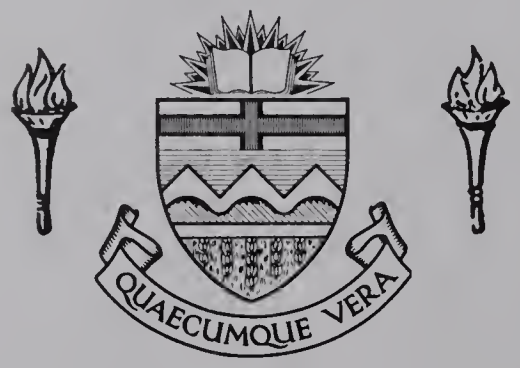

THE UNIVERSITY OF ALBERTA

MEASUREMENTS OF TANGENTIAL MOMENTUM EXCHANGE BETWEEN A RAREFIED GAS AND A SOLID SURFACE

by

GARRY BENSON, B.Sc. (Alberta)

A THESIS

SUBMITTED TO THE FACULTY OF GRADUATE STUDIES

IN PARTIAL FULFILMENT OF THE REQUIREMENTS FOR THE DEGREE

OF MASTER OF SCIENCE

DEPARTMENT OF MECHANICAL ENGINEERING

EDMONTON, ALBERTA

April 1968

UNIVERSITY OF ALBERTA

FACULTY OF GRADUATE STUDIES

The undersigned certify that they have read, and recommend to the Faculty of Graduate Studies for acceptance, a thesis entitled "MEASUREMENTS OF TANGENTIAL MOMENTUM EXCHANGE BETWEEN A RAREFIED GAS AND A SOLID SURFACE" submitted by GARRY BENSON in partial fulfilment of the requirements for the degree of Master of Science.

ABSTRACT

An apparatus was constructed to measure tangential momentum accommodation coefficient (σ) of a rarefied gas on a solid surface. A highly polished steel sphere (3/8 inch diameter) was magnetically suspended in a vacuum system where it could be accelerated to a high rotational speed and then allowed to coast freely. Deceleration due to tangential momentum exchange by a test gas admitted to the chamber was measured, using an optical technique, to obtain numerical values for σ.

Sublimation filaments were incorporated into the system to allow deposition of a thin film of silver on the surface of the sphere immediately prior to deceleration tests.

Tests were conducted on various surface conditions with major interest on this freshly deposited film of silver. Results were obtained for nitrogen, helium, and argon at test pressures ranging from 10^{-4} to 10^{-2} torr. Nitrogen and argon exhibited σ's ranging primarily between 0.85 and 0.98 depending on the surface condition. Helium displayed accommodation coefficients as low as 0.3 on a freshly deposited silver film and as high as 0.95 on a silver film which had several days to acquire a layer of contamination. These lower measured accommodation coefficients confirm the existence of some non-diffuse reflection, perhaps specular or specularly directed diffuse.

ACKNOWLEDGEMENTS

I am grateful to Dr. D.J. Marsden for providing the opportunity to undertake this project and for his guidance and patience during the various phases of the thesis.

The apparatus included a sizeable amount of electrical engineering and electronics which worked very successfully. This was due to the design and efforts of Don MacFarlane.

Thanks must go to the staff members of the Mechanical Engineering Shop for the construction of the apparatus and for their continued help during the tests.

The assistance and patience of Peter Lea from the Glass Shop was also much appreciated.

This project was financially supported by the National Research Council and the University of Alberta.

TABLE OF CONTENTS

PAGE

NOTATION

c_n	random thermal gas velocity, n = 1,2,3.
c_m	most probable molecular speed.
	$= \sqrt{2RT}$
f_e	Maxwell's Velocity Distribution Function for a gas in equilibrium.
I	moment of inertia about vertical axis of sphere.
k	Boltzmann's constant.
Kn	Knudsen Number.
m	mass of a molecule.
n	molecule number density.
P_G	chamber pressure as indicated from ionization gauge.
P_S	chamber pressure as indicated from deceleration of sphere.
$(P_S)_{cor}$	P_S corrected for residual drag.
R	gas constant per unit mass of gas.
R_s	sphere radius.
r, ϕ	spherical co-ordinates.
t	time.
T	absolute gas temperature.
τ_i	impinging tangential momentum.
τ_r	reflected tangential momentum.
u	gas macroscopic velocity.
W	drag torque on sphere.
$\underline{x}$	position vector.

α	angular deceleration of sphere.
$\underline{\xi}$	molecular velocity vector.
	$= \xi_1 + \xi_2 + \xi_3$
σ	Tangential Momentum Accommodation Coefficient.
σ(gas)	Tangential Momentum Accommodation Coefficient for different gases - N_2, A, He.
ρ	Mass density of sphere.
μ	Micron = 10^{-3} torr (mm Hg pressure).
ω	Angular velocity of sphere.

LIST OF FIGURES

LIST OF TABLES

CHAPTER I

INTRODUCTION

The experimental data presented in this thesis deals with the exchange of tangential momentum between a gas under free molecular flow conditions (rarefied) and a solid surface.

The free molecule flow regime of gas dynamics is one in which the mean free path of molecules in the gas is large compared to a typical dimension of the solid surface. The impinging molecules are thus representative of the gas with negligible modification by collisions with reflected molecules.

Free molecular flow conditions exist in the atmosphere above an altitude of approximately 80 miles. Tangential momentum exchange between this ambient atmosphere and low orbiting earth satellites will be an important factor in the decay of orbits and control of such vehicles.

Under free molecular flow conditions, the tangential momentum of molecules incident on a solid surface can be easily calculated using the kinetic theory of gases. However, in order to complete the calculation of momentum exchange, it is necessary to know the momentum carried away by the reflected molecules. This would require a detailed knowledge of the interaction taking place at the surface which is not currently available.

Reflection at the surface can be thought of as being between the extremes of diffuse reflection and specular reflection. Diffuse reflection occurs at a rough or contaminated surface whereas specular reflection

is conceived as a mirror-like reflection from a "molecularly smooth" surface.

In this study, the conventional empirical approach has been taken in which an accommodation coefficient has been used to relate the average unknown reflected tangential momentum to the average known incident tangential momentum. The primary concern of this project was to gather experimental values of this coefficient (σ).

Very little experimental data exists on momentum accommodation coefficients (1), especially for momentum exchange at "molecularly smooth" surfaces. This is primarily because a "molecularly smooth" surface is very difficult to produce in a laboratory. Saltzburg and Smith (2) were able to obtain gas scattering data on a relatively smooth and homogeneous surface by simultaneously depositing metal onto the target. As reported in (3), they subsequently found that a fresh deposit of silver remained clean for a considerable time following the termination of deposition. A similar process was adopted in this work with silver being sublimated onto the surface of the rotating sphere prior to each measurement of σ.

Nitrogen was chosen as the main test gas although argon and helium were also used.

CHAPTER II

THEORY

Although man has been speculating on the nature of gases since the time of the early Egyptians, the foundations of the kinetic theory of gases were not laid until the work of Gassendi in the 17th century (4). He assumed gas to consist of widely separated atoms similar in substance although varying in size and form, to move in all directions through empty space, and to be devoid of all qualities except absolute rigidity.

Various scientists worked on the subject during the next 200 years but the most significant breakthrough was made by J.C. Maxwell in 1859 when he presented his famous law of distribution of velocities. In the following 20 years, the subject was developed by Maxwell and Clausius to a state which is, with few changes, accepted today.

Modern kinetic theory defines an ideal gas as a group of molecules, each moving on its own independent path, entirely uncontrolled by forces from the other molecules. The speed and direction of the molecule may be altered abruptly, however, whenever it collides with another molecule or strikes the walls of its container.

The most commonly used analogy to a gas molecule is a minute billiard ball. It follows that a two dimensional analogy of a gas might be a billiard table containing a large number of balls moving in random directions with random velocities. This hard sphere analogy gives an accurate description of the kinetic theory of monatomic gases. It is also satisfactory for polyatomic gases in most cases. It can not

account for energy exchange between the translational and internal modes of energy during collisions.

It is interesting to note that the kinetic theory predicts the behaviour of a gas as a whole on a statistical mechanics basis while remaining in almost complete ignorance of the properties and behaviour of the molecules of which it is composed (5).

2.1 Classification of Flow Regimes

There are three different gas regimes which are characterized by the mean free paths of the molecules. These regimes are generally specified by three range values of a dimensionless parameter called Knudsen Number (Kn), defined as the ratio between the mean free path and a characteristic dimension (the sphere diameter in this case).

The three regimes with corresponding Knudsen Numbers are outlined below. This is only a rough guide as the transition is gradual.

Free molecule flow	$Kn > 1$
Continuum	$Kn < 0.01$
Transition	$.01 < Kn < 1$

2.2 Maxwell Distribution Function

Although the kinetic theory picture of a gas has been previously mentioned, the assumptions pertaining to the specific case of a rarefied gas are repeated below (6):

(a) The gas molecules are considered as hard elastic spheres with no intermolecular forces except on contact.

(b) Internal degrees of freedom of a diatomic molecule (N_2) have no effect on momentum exchanged during collision with other molecules or solid surfaces. (Hard sphere model).

(c) Molecular chaos is assumed as originally introduced by Boltzmann.

(d) Since the gas is rarefied, the duration of a collision is assumed much less than the time of transit between encounters i.e. molecular diameter is very small compared to the mean free path.

The above assumptions plus the fact that there are a very large number of molecules per unit gas volume, even when rarefied, enables a statistical prediction of the molecular positions and velocities.

In general, macroscopic properties such as momentum and energy transport for a gas at rest and in equilibrium, can be written in terms of Maxwell's velocity distribution function $f_e(\underline{\xi},\underline{x},t)\ d\underline{\xi}\ d\underline{x}\ dt$. f_e is defined as the number of molecules in the physical volume $d\underline{x}$ around $\underline{x}$ having velocities within $d\underline{\xi}$ about $\underline{\xi}$, and has the established form (6):

$$f_e(\underline{\xi},\underline{x},t)\ d\underline{\xi}\ d\underline{x}\ dt = \frac{n}{(2\pi RT)^{3/2}}\ \exp(-\underline{\xi}^2/2RT) \qquad (1)$$

where f_e = number of molecules with velocity $\underline{\xi}$ in gas at rest and in equilibrium. (Maxwellian Distribution Function)

n = molecular number density.

R = gas constant per unit mass of gas.

T = absolute gas temperature.

Maxwell originally proved this law (5). However, his proof is considered incomplete because he did not support his assumption of molecular chaos. A more acceptable proof was presented by Boltzmann and Lorentz (5).

2.3 Tangential Momentum

A number of gas properties can be derived from the above function. The most pertinent to this work is the transfer of tangential momentum from a gas in equilibrium across an area dA which is moving with tangential velocity (-u):

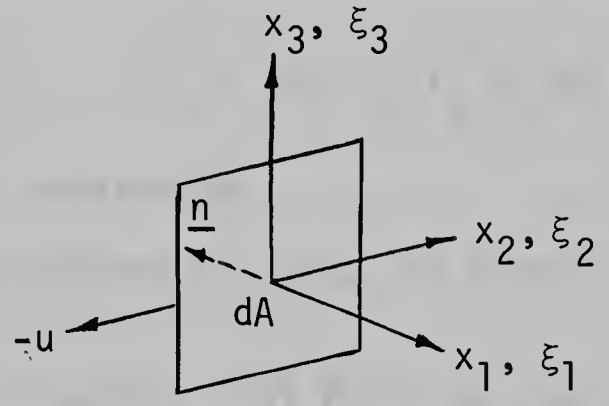

ξ_1, ξ_2, ξ_3 are molecular velocity components in directions x_1, x_2, x_3 respectively. $\underline{n}$ is a unit vector in the negative x_1 direction.

It is more convenient to consider the gas moving at a velocity (+u) relative to dA. A new velocity coordinate system moving with the gas macroscopic motion can then be chosen such that:

$$\begin{aligned} \xi_1 &= c_1 & d\xi_1 &= dc_1 \\ \xi_2 &= c_2 + u & d\xi_2 &= dc_2 \\ \xi_3 &= c_3 & d\xi_3 &= dc_3 \end{aligned} \qquad (2)$$

where c_1, c_2, c_3, are components of the random thermal gas velocity.

The number of molecules which hit dA from the x_1 direction during dt would be equal to the number of molecules, which at the beginning of dt, lie within a volume standing on dA as base and having height $\underline{\xi} \cdot \underline{n}\ dt = \xi_1\ dt$ and hence volume $\xi_1\ dA\ dt$.

From kinetic theory, the number of molecules in this elemental physical volume having velocities within $d\underline{\xi}$ about $\underline{\xi}$ would be:

$$\xi_1\ f_e\ d\underline{\xi}\ dA\ dt \tag{3}$$

This expression gives the number of molecules (with velocity $\underline{\xi}$) that hit dA in time dt. To obtain the impinging tangential momentum, τ_i, due to these $\underline{\xi}$ molecules, it is necessary to multiply by $m\xi_2$ so that,

$$\tau_i = m\xi_1\ \xi_2\ f_e\ d\underline{\xi}\ dA\ dt \tag{4}$$

where m = mass of a molecule.

Substituting equations (2) into (4) gives

$$\tau_i = mc_1(c_2 + u)\ f_e\ dc_1\ dc_2\ dc_3\ dA\ dt.$$

Now using Maxwell's law for f_e and integrating over all velocity ranges to account for all molecules which hit dA:

$$\tau_i = m \int_0^\infty c_1\ f_e(c_1)dc_1 \int_{-\infty}^{\infty} (c_2 + u)\ f_e(c_2)\ dc_2 \int_{-\infty}^{\infty} f_e(c_3)\ dc_3\ dA\ dt$$

$$= \frac{n\ m\ c_m\ u}{2\sqrt{\pi}} \tag{5}$$

where $c_m = \sqrt{2RT}$, the most probable molecular speed.

2.4 Surface Interaction Models

As mentioned in the introduction, the two basic theoretical models of the gas-solid surface interaction are diffuse reflection and specular reflection. In diffuse reflection, the molecules are assumed to be adsorbed and later re-emitted with a Maxwellian Velocity Distribution. The surface may be so cavernous and irregular that the molecules strike many times before escaping or the interaction may be more like a process of molecular condensation and later evaporation. Either way, the molecule looses all memory of its original condition and is re-emitted with a Maxwellian Velocity Distribution corresponding to some mean temperature value. This mean temperature may be equal to the surface temperature (perfectly diffuse or completely accommodated reflection) or equal to some value between the incident gas temperature and surface temperature.

Specular reflection on the other hand, describes the situation in which the normal velocity component of the incident molecules is reversed in direction but unchanged in magnitude, while the tangential component remains unchanged with regard to both magnitude and direction. This mirror-like reflection results in no temperature accommodation as the reflected molecules have not given up any of their kinetic energy.

Some recent work on momentum accommodation coefficients (for example, reference 1) utilizes a model whereby a fraction of the incident gas molecules are reflected diffusely and the remainder are reflected specularly. This model was originally suggested by Maxwell.

Another model, quasi-specular or lobular reflection, is suggested by molecular beam experiments to describe scattering phenomena on

clean metal surfaces (3, 7, 13). In this model, the gas molecules are reflected with a lobular distribution about some central axis which may or may not coincide with the specular axis.

It must be conceded that the reflection process of a rarefied gas on a clean metal surface is generally not well understood. An accurate means of defining and controlling the surface together with a satisfactory technique of analyzing the reflected molecules are the major obstacles. Many current experimental and theoretical studies are centered on this problem as evidenced by the number of papers on Gas-Surface Interactions in reference (13).

2.5 Tangential Momentum Accommodation Coefficient

The tangential momentum accommodation coefficient, σ, is defined as:

$$\sigma = \frac{\tau_i - \tau_r}{\tau_i} \tag{6}$$

where τ_i = incident tangential momentum (equation 5)

τ_r = reflected tangential momentum

This accommodation coefficient is an indication of the two extreme reflection processes in that $\sigma = 1.0$ for diffuse reflection ($\tau_r = 0.0$) and theoretically, $\sigma = 0.0$ for specular reflection ($\tau_i = \tau_r$). For values of $\sigma < 1.0$, however, no direct conclusion as to the appropriate model can be determined except that the reflection is not diffuse. Probably the best model for $\sigma < 1.0$ is the quasi-specular lobe reflection.

Since this experiment furnishes no details on the reflection model, σ is evaluated as an empirical coefficient without further reference to reflection model except that it is not diffuse when $\sigma < 1.0$.

2.6 Derivation of σ in Terms of Sphere Deceleration

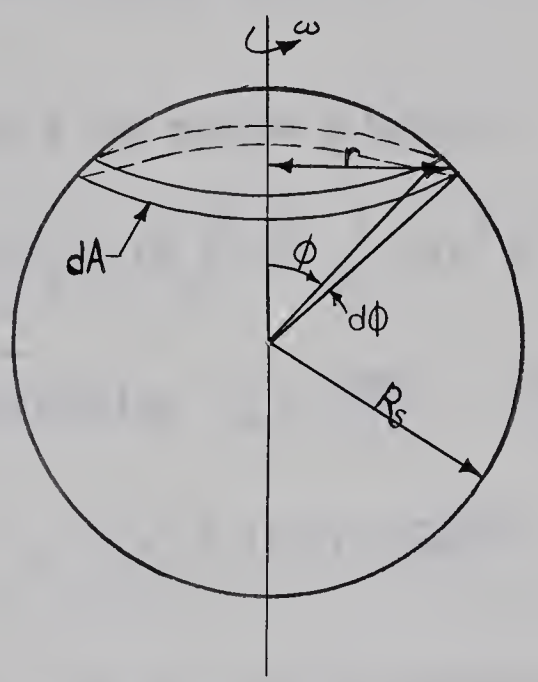

The drag torque, W on a rotating sphere (see above diagram) due to the transfer of tangential momentum from the surrounding rarefied gas is given by

$$W = \int_{\text{area}} r(\tau_i - \tau_r)\, dA.$$

Using the definition of $\sigma = (\tau_i - \tau_r)/\tau_i$;

$$W = \int_{\text{area}} r\, \tau_i\, \sigma\, dA$$

Referring to the above diagram,

$r = R_s \sin \phi$, where R_s is the radius of the sphere,

$dA = 2\pi(R_s)^2 \sin \phi \, d\phi$,

$u = R_s \omega \sin \phi$, so that substitution into equation (5) gives

$\tau_i = (m \, n \, R_s \, \omega \, c_m \sin \phi)/2\sqrt{\pi}$.

The total drag torque W can now be obtained:

$$W = m \, n \, \omega \, c_m \, \sigma \, (R_s)^4 \sqrt{\pi} \int_0^{\pi} \sin^3 \phi \, d\phi$$

Integrating and substituting $c_m = \sqrt{2RT} = \sqrt{2kT/m}$ and $n = P/kT$:

$$W = \omega\sigma \, P \, (R_s)^4 \, (4/3) \sqrt{2\pi m/kT}$$

The moment of inertia about the vertical axis of the sphere is given $I = (8/15) \, \rho\pi(R_s)^5$ where ρ = mass density of the sphere. Using this, it is possible to calculate the deceleration $(-\alpha)$:

$$-\alpha = W/I = (5 \, \omega \, \sigma \, P/\rho \, R_s) \sqrt{m/2\pi kT}$$

As the experimental apparatus records angular velocity change $(\omega_0 - \omega)$ over a corresponding time interval $(t - t_0)$, it is more convenient to express the above equation as follows:

$$-\int_{\omega_0}^{\omega} \omega^{-1} \, d\omega = \int_{t_0}^{t} (5 \, \sigma \, P/\rho \, R_s) \sqrt{m/2\pi kT} \, dt$$

Integrating and rearranging

$$\sigma = \frac{\rho R_s \sqrt{2\pi kT/m} \ln \omega_0/\omega}{5P(t - t_0)} \tag{7}$$

As this project involved the measurement of sphere deceleration rates for various pressures, measured on an ionization gauge, it is convenient for future discussions to express equation (7) as

$$\sigma = \frac{P_S}{P_G} \tag{8}$$

where $$P_S = \frac{\rho R_s \sqrt{2\pi kT/m} \ln \omega_0/\omega}{5(t - t_0)} \tag{9}$$

and $P_G = P$.

P_S is simply the chamber pressure obtained from the deceleration of the sphere and P_G is the absolute chamber pressure obtained from the calibrated ionization gauge.

CHAPTER III

APPARATUS

3.1 General Vacuum Equipment

The general arrangement and some details of the vacuum system are shown in figures 1 and 2.

All major components in contact with the ultra high vacuum region were stainless-steel or glass. The glass was necessary to facilitate the use of photodiodes and enable easy operation of the filaments. The main test chamber was fitted with bakeable Varian flanges and copper gaskets.

The bakeable portion, shown in figure 1, was baked at 325°C with a temperature regulated Marinite oven. A roughing pressure in the range of 10μ was produced with a Linde 13X molecular sieve sorption pump. This pump was capable of three or four uncontaminated roughings before requiring a bakeout cycle.

A General Electric 25 L/S triode ion pump produced an ultimate pressure of approximately 5×10^{-9} torr.

The inner dashed line of figure 1 represents the protection box consisting of 1/16 inch mild steel sheeting with a 3/4 inch plywood backing. The bursting speed of the 3/8 inch diameter sphere was estimated to be slightly over 1,000,000 RPM using Chree's method (8). The maximum operating speed of the sphere was approximately 170,000 RPM which allowed a safety factor of about 6.

The mild steel in the protection box was also intended to provide magnetic shielding. However, early tests proved it insufficient and a cylinder of .004 inch conetic alloy around the sphere and suspension system was also used. Figure 3 shows the bare apparatus while figures 4 and 5 show the conetic magnetic shielding and mild steel protection box respectively.

Pressure gauges included a Varian Millitorr ionization gauge in the test chamber and a Pirani gauge on the roughing line. The ionization gauge was designed to operate from 10^{-5} torr to 1 torr and was calibrated in situ as discussed later. An indication of the ultimate pressure was obtained from the ion pump current.

The spherical rotors consisted of SAE 52100 chrome alloy steel ball bearings with a yield strength of approximately 200,000 psi. These grade 2 spheres were highly polished so that their 3/8 inch diameters were accurate to within .000002 inches.

These spheres were handled with caution so that their surfaces would not be etched by the moisture etc, on hands. Various chemical and electrolytic polishing methods were tested and were found to be unsuccessful in making the surface smoother. The spheres were carefully washed in carbon tetrachloride, distilled water, and dried before being inserted into the vacuum system.

The test gas inlet line included both a liquid N_2 trap and a selective nickel getter as shown in figure 6. The trap would eliminate any condensible impurities and the nickel getter would chemisorb CO, H_2, and O_2 leaving a purified test gas. This nickel filament was approximately 4 inches long and .020 inches in diameter.

Two silver filaments were fitted into the glass adapter next to the sphere. These 99.999% pure silver filaments (3/4 inches long and .015 inches in diameter) could be heated with an electric current so that silver molecules were deposited on the surface of the sphere.

3.2 Electronic Components

The instrument panel is shown in the photograph of figure 7. A discussion of the individual components follows below.

3.2.1 Magnetic Suspension System

A block diagram of the magnetic suspension system is shown in figure 8 with the pertaining circuit diagram in figure 8a.

When suspended, the sphere was positioned midway in the light beam between the light bulb and the H-35 photodiode. Any upward movement would allow more light to enter the photodiode and a downward movement would decrease this amount of light. The current in the suspension magnet was regulated by the photodiode and amplifier circuit in such a manner that the vertical sphere movement would be counteracted with an opposing change in the supporting magnetic field. With careful adjustment of the circuit to avoid oscillation or "hunting", the sphere would come to an equilibrium position with virtually no vertical movement.

The suspension magnet consisted of 1325 turns of #24 magnet wire with a moveable pendulum type core mounted on a short length of .015

inch diameter steel wire (see figure 2). This core was immersed in light SAE 10 W oil which, because the sphere and core were magnetically coupled, effectively damped the horizontal motion of both.

Figure 2 also shows the moveable glass cup fixture which encloses a small iron cylinder. This fixture could be moved vertically with an external magnet so that the sphere could be raised into position.

3.2.2 Counting System

Referring again to the block diagram of figure 8, another H-35 photodiode was aimed at the reflection of the light bulb on the surface of the suspended sphere. A small sandblasted scratch approximately 1/4 inch long by .010 inch wide interrupted the light signal once each revolution. This signal was amplified (figure 8b) and shaped (figure 8c) so that it could be counted by the model 6 B45 Atec digital counter and recorded on a model 562A Hewlett Packard digital recorder.

At higher RPM, the photodiode signal became very weak and barely distinguishable from the noise pickup in the system. Under these conditions, it was necessary to compare the final shaped signal with the signal received directly from the photodiode. This was done with a CRT oscilloscope. By adjusting the triggering level and pulse length of the pulse shaping circuit, the final counting signal could be made to correspond to the photodiode signal regardless of noise pickup or wave shape. At speeds above 200,000 RPM, however, the signal was too small to be counted.

Figure 9 is a photograph of the oscilloscope screen when the

sphere is rotating at speeds under 30,000 RPM. The photodiode signal is shown on the top trace, and the final shaped signal is shown on the bottom trace as the output of the Monostable Multivibrator. The middle trace shows the signal at the output of the Schmitt Trigger before being modified by the Monostable Multivibrator.

Figure 9a is similar to figure 9 with the exception that the sphere is rotating at a much higher RPM. Here, the system noise interferes with the photodiode signal and is strong enough to be counted by the Schmitt Trigger. The Monostable Multivibrator eliminates the inaccurate noise counts, however, and furnishes a final counting signal which corresponds exactly to the actual RPM of the sphere.

3.2.3 Rotational Driving System

The schematic diagram of figure 10 shows the essential features of this system. Four field coils wound on a ferrite core structure were positioned horizontally around the glass container.

A phase shifter, powered by a variable oscillator, produced two voltage signals which were 90° out of phase. These signals were applied to drive amplifiers which provided power for the field coils. The sphere was thus accelerated in a manner similar to the armature of an induction motor. The system was designed for an oscillator frequency of 8250 cps which would give the sphere a maximum speed of 495,000 RPM. However, because of counting difficulties, the sphere was not operated above 200,000 RPM.

This system would accelerate the sphere at a rate of approximately 3000 RPM/min.

3.2.4 Power Supplies

The power supply system is shown schematically in figure 11. Two well regulated power supplies were used to operate the various electronic components of the apparatus. An auxiliary power source composed of four wet cell batteries with diode switching networks would keep the sphere suspended in case of a power failure during a test.

The silver and nickel filaments were operated with a 0-18 V, 0-45 Amp DC power supply.

CHAPTER IV

PROCEDURE

4.1 General Procedure

Data was generally obtained with the following procedure: A more detailed discussion of the various tests follows later.

(a) Suspend and accelerate the sphere to approximately 150,000 RPM then switch off the rotational driving force.

(b) Outgas the ionization gauge (2 to 5 min.).

(c) Fill cold trap and deposit a new layer of nickel in the selective getter.

(d) Measure residual drag with the system at ultimate pressure (low 10^{-7} torr range to 10^{-9} torr range) with the ionization gauge off.

(e) Turn on the ionization gauge.

(f) Shut off the ion pump.

(g) Admit test gas, deposit silver, record pressure and shut off ionization gauge.

(h) Record revolutions per second (at constant pressure) every 10 seconds for 100 to 1000 seconds depending on the pressure.

(i) Turn on ionization gauge to check pressure at the end of the test.

(j) Readmit test gas to a slightly higher pressure, deposit silver, measure this new pressure with ionization gauge, and then shut off gauge.

(k) Repeat steps (h) to (k).

(l) After highest pressure tested, start ion pump (ionization gauge off), evacuate system to ultimate pressure, and remeasure residual drag. The speed of the sphere had usually decreased to about 110,000 RPM.

(m) Reverse polarity in the driving coils, decelerate sphere back to zero RPM, and drop it back into the glass cup.

All normal tests were conducted at pressures in the free molecule flow regime which, as determined by the straight line portion of figure 12, had an upper limit of approximately 2×10^{-2} torr.

4.2 Residual Drag

At pressures below the 10^{-5} torr range, factors other than gas pressure become important in the deceleration of a magnetically suspended coasting sphere. Fourteen possible "residual drag" factors have been cited in the paper by J.W. Beams (9). Probably the three major decelerating factors in this project were:

(a) Magnetic poles in the rotor not exactly coincident with the axis of rotation.

(b) Stray magnetic fields perpendicular to the axis of rotation.

(c) Building or other vibrations (see figure 13) causing the magnetic flux from the suspension magnet to change in the sphere.

All these factors would cause eddy currents in the sphere which in turn would cause a loss of energy and a deceleration of the sphere.

Effects (a) and (b) were minimized by first carefully demagnetizing the sphere with a 60 cps coil demagnetizer and then shielding it with a steel box plus magnetic shielding alloy as discussed previously. Building vibrations were damped by mounting the whole apparatus on two inches of foam rubber and running the tests after midnight when activity in the building was at a minimum. The residual drag was not eliminated entirely, however, so that measurements of P_S below the 10^{-3} torr range required a small correction.

This was obtained from the sphere deceleration measured at the ultimate pressure where drag due to the surrounding gas could be neglected. This residual drag is dependent primarily on the RPM of the sphere (figure 14) and R_s, the radius of the sphere. Any variation in R_s would be extremely small because all tests were conducted at room temperature which was essentially constant. Consequently the expression for P_S in equation (9) could be easily corrected for residual drag as shown in the following expression:

$$(P_S)_{cor} = \frac{\rho R_s \sqrt{2\pi kT/m}}{5} \left[\frac{\ln \omega_o/\omega}{t - t_o} - \left(\frac{\ln \omega_o/\omega}{t - t_o}\right)_{RD}\right] \qquad (10)$$

The subscript RD denotes the residual drag correction term. As outlined in the Procedure, this quantity was measured both before and after each group of tests. Using an approximate straight line variation with RPM, the proper correction could be applied to each test measurement of σ.

Referring again to figure 14, the pressure equivalent of residual drag is seen to vary inversely with the RPM of the sphere. This

surprizing phenomenon is not easily explained and is expected to be a result of the frequency response of the steel in the sphere. An interesting electrical engineering analysis could be based on this observation.

4.3 Calibration of Ionization Gauge

The largest experimental error was expected to be in the measurement of pressure by the ionization gauge. This gauge was consequently calibrated in situ both before and after the collection of experimental data.

The first calibration was undertaken immediately after the bakeout using a sphere which had accidentally become oxidized by a bakeout with insufficient rough pumping. The second calibration, at the end of the tests, was undertaken with a sandblasted sphere. The two surfaces are shown in the microscope photographs of figures 15 and 16. The results from the sandblasted sphere were used in the calculation of σ as this surface seemed more uniformly rough.

The reflection of molecules from this rough surface would certainly be diffuse and thus $\sigma = 1.0$. This fact enables an absolute calibration of the chamber pressure based on the deceleration of the sphere. Using primed letters to denote the quantities measured with this sandblasted sphere and incorporating the residual drag correction, equation (8) can be rewritten

$$(P_S')_{cor} \equiv P_G \tag{11}$$

This method of using the diffuse reflection from a magnetically suspended sphere to measure absolute pressure has been established previously (10,11). The results of the calibration using the sandblasted sphere are shown in figure 17.

The procedure required changing spheres which meant venting the system to atmospheric pressure. The precaution taken here was to purge the system to atmospheric pressure first with dry nitrogen and then exchange spheres as quickly as possible. The system was consequently open to the atmospheric air for only three to four minutes. The ultimate pressure obtained immediately after the change was equal to the pressure immediately before indicating little or no contamination entered the system. The electrodes of the ionization gauge apparently adsorbed some gases, however, as it operated erratically at low pressures immediately following this high pressure change-over stage. These gases desorbed quite quickly and only the first in a series of readings was affected.

Also, the filament of the gauge was close enough to the container walls to cause heating and outgassing if operated continuously. For this reason, the gauge was shut off during the bulk of any test and was operated for a short time only at the beginning and end of each test.

The counting signal from the sandblasted sphere was obtained from a short, thin strip of shiny metal which had been left unsanded.

4.4 Measurement of σ

The procedure for measuring σ was similar to that of calibrating the ionization gauge. A highly polished sphere was used instead of the rough sphere and silver was deposited onto the surface prior to each constant pressure test. This was accomplished by first outgassing the filament for a few seconds and then heating it with increased current to a white hot glow for 5 to 20 seconds. Sublimation of silver was indicated by the blackening of the surrounding glass. Immediately after the silver had been deposited, the deceleration of the sphere was measured along with the chamber pressure as indicated by the ionization gauge. After correcting P_S for residual drag, σ could be easily calculated as follows:

$$\sigma = \frac{(P_S)_{cor}}{P_G} \tag{12}$$

CHAPTER V

RESULTS AND DISCUSSION

5.1 Results and Discussion

5.1.1 Preliminary Measurement of σ with Nitrogen on Plain Polished Steel

Test values of $\sigma(N_2)$ with pertaining data are given in table 1. Figure 18 shows a plot of $\sigma(N_2)$ versus pressure. The sphere was thoroughly washed with carbon tetrachloride, alcohol and distilled water before being inserted into the vacuum system. However, silver was not deposited onto the surface of the sphere and it was not treated in any other way prior to testing.

The average value of $\sigma(N_2)$ was found to be .88 giving a strong suggestion of some non-diffuse reflection.

5.1.2 Measurement of σ with Nitrogen on Freshly Deposited Silver

Tables 2 and 2a show the results of these tests which are also plotted in figure 18. The sphere which was used in the plain steel test was used throughout all σ measurement tests. The procedure here included the deposition of silver onto the sphere's surface prior to each reading at each different test pressure. (Silver does not chemisorb N_2, He or A. See reference 12). The average value of $\sigma(N_2)$ is approximately .93 which is slightly higher than that measured for plain

polished steel. This would suggest that the reflection from the freshly deposited silver surface was more diffuse than that from the plain polished steel surface. The opposite effect was expected, namely that the silver film would exhibit a less diffuse reflection. The fact that silver was deposited at the relatively high test pressures and not at the ultimate pressure may have caused the silver film to be rougher on a microscopic scale.

5.1.3 Measurement of σ for Helium on Freshly Deposited Silver

The test is summarized in tables 3 and 3a and the resulting values of σ(He) are plotted versus absolute pressure in figure 19.

The average value of σ(He) is approximately .43. This generally lower value complies with the established trend that lighter noble gases yield smaller values of both normal and tangential accommodation (13).

As can be seen in figure 19, σ(He) seems to be slightly dependent on pressure. There are two possible considerations which may have caused this:

(a) Silver film may be rougher when deposited at higher pressures. This phenomenon has been observed in the operation of getter pumps where the required rougher films are produced by evaporation in an inert gas (14).

(b) The adsorption of contaminants on the surface may have caused this pressure dependence of σ(He), as was the case in some thermal accommodation measurements (15).

5.1.4 Measurement of σ with Argon on Freshly Deposited Silver

The results of this test are tabulated in table 4 and plotted in figure 20. The average value of $\sigma(A)$ is .95 which is high relative to previous tests. Similarly high values have been measured, however, in the normal momentum accommodation of low energy argon molecular beams on contaminated "engineering" surfaces (16).

This test was incomplete due to a leaking needle valve in the argon inlet line.

5.1.5 Measurement of σ with Nitrogen on Aged Silver

After leaving the silvered sphere under ultra high vacuum conditions (10^{-9} torr range) for two days, it was again tested without further deposition of silver. The results are shown in table 5 and are plotted versus pressure in figure 18.

It was expected that the silver, during this dormant period, would adsorb some gas molecules which would cause an increase in $\sigma(N_2)$. However, a noticeable difference was not observed, suggesting that either the surface did not become contaminated during its dormant period or that it was already contaminated during the earlier tests.

5.1.6 Measurement of σ with Helium on Aged Silver

Table 6 is a tabulation of the experimental parameters measured in this test. Figure 19 shows the variation of $\sigma(He)$ versus pressure.

Contrary to $\sigma(N_2)$ measurements, σ(He) for this test was significantly higher (.89 average) than σ(He) measured on the fresh silver film (.43 average). This large difference indicates some change in the surface condition between the first and later tests. Further, it provides evidence that the surface was relatively clean in the first case but adsorbed gas layers in the interim period. The absence of a similar increase in the previous $\sigma(N_2)$ measurements would suggest that the adsorption took place during or following this test with N_2. Other factors contributing to this inconsistency may be the large difference in mass between He and N_2 molecules and perhaps differences in molecular attractive forces.

5.1.7 Measurement of σ with Argon on Aged Silver

The results of this test are shown in table 7 and values of σ(A) are plotted versus pressure in figure 20.

This data is incomplete so that no direct conclusions can be drawn. The silver surface was apparently still clean enough to cause some non-diffuse reflection of the argon molecules.

5.2 Estimate of Accuracy

5.2.1 Gas Temperature Effects

The substitution of P_G from equation (11) into equation (12), results in the relationship:

$$\sigma \equiv \frac{(P_S)_{cor}}{(P_S')_{cor}}$$

where $(P_S)_{cor}$ was measured with the smooth surface test sphere and $(P_S')_{cor}$ was measured with the sandblasted calibration sphere.

Utilizing equation (10) with primed letters denoting quantities measured with the sandblasted sphere,

$$\sigma \equiv \frac{\rho R_s \sqrt{T/m} \left[\frac{\ln \omega_o/\omega}{t - t_o} - \left(\frac{\ln \omega_o/\omega}{t - t_o}\right)_{RD}\right]}{\rho' R_s' \sqrt{T'/m'} \left[\frac{\ln \omega_o'/\omega'}{t' - t_o'} - \left(\frac{\ln \omega_o'/\omega'}{t' - t_o'}\right)_{RD}\right]}$$

T and T' represent gas temperature during the σ measurement tests and calibration tests respectively.

All tests were conducted at room temperature with similar testing procedures. This included a warm-up period of at least one hour which would ensure equilibrium apparatus temperature. Consequently, it is probable that T = T' and that σ is independent of temperature.

The actual value of T would be equal to the average wall temperature which unfortunately varied from 580°R in the immediate vicinity of the light bulb to room temperature 538°R at the extremities of the container. The assumption of equilibrium gas with Maxwellian Velocity Distribution may not be strictly correct in view of this variation of wall temperature.

5.2.2 Estimation of Experimental Errors Due to ω, ρ, R_s, t

The experimental errors in these four factors are assumed to be:

$$\Delta\omega = .00005\ \omega$$

$$\Delta\rho = .001\ \rho$$

$$\Delta R_s = .000005\ R_s$$

$$\Delta t = .001\ t$$

For approximate typical values of ω = 2000 rps, ρ = 8 gm/cc, R_s = 1 cm, σ = 1.0, and t = 300 sec, the resulting error in σ caused by these four factors is approximately .002 or .2%.

5.2.3 Estimation of Error Due to P_G

The experimental accuracy of the ionization gauge was estimated from the calibration test obtained with the sandblasted ball. Referring to figure 17, the abscissa of the calibration curve was calculated from the deceleration of the sphere. Assuming the gas temperature to be constant throughout the test, this calculation would be reasonably accurate (± .2%) and at least linear. Thus the scatter of the experimental points was attributed to the ionization gauge and this scatter was used to give an estimation of the accuracy of the ionization gauge. These points varied over a range of about 7% in the low part of any gauge decade to 2-3% in the higher regions. Experimental data collected for pressures below approximately 1.5 in any decade was rejected as the gauge was very inaccurate in this region.

5.2.4 Total Estimated Experimental Errors

Except for a few erratic readings, the measurements of σ are estimated to vary in accuracy between 7.1% in the low part of any pressure decade to 3.1% in the higher part of any pressure decade. The major source of this error was of course the ionization gauge.

5.3 Other Possible Sources of Errors

5.3.1 Contamination

The hot filament of the ionization gauge may have been a source of contamination both from the filament itself and indirectly from the heated walls of the stainless-steel container. Contamination in the form of CO, CO_2, H_2, O_2 and any heavy hydrocarbons could have two effects on this experiment. First, the surface of the sphere may adsorb some of these molecules which would tend to cause a more diffuse reflection. Secondly, the pressure as recorded by the ionization gauge may be slightly in error. (Although this would require a large amount of contamination).

A means of residual gas analysis would have been helpful in resolving the question of gauge contamination.

5.3.2 Pressure During Measurement of σ

The ionization gauge pressure at the end of each deceleration reading was usually 1% to 10% higher than the pressure observed at the

beginning of the reading. This was assumed to result from outgassing during the test and an average of the two pressures was used to calculate σ. Averaging these two pressure measurements may have incorporated an error, however, because the outgassing rate may not have been constant during the test.

5.3.3 Abnormal Deceleration of Sphere

As briefly mentioned before, any vibration of the apparatus would cause a change in the magnetic flux through the sphere. This would set up eddy currents which would constitute an energy loss and decelerate the sphere. Figure 13 shows the result of someone walking and jumping on the floor beside the apparatus.

The sphere was also very sensitive to temperature changes, as demonstrated in figure 21. During low pressure deposition of the silver, radiation from the hot filament apparently heated the sphere slightly. This caused it to expand which in turn increased its deceleration. When the hot filament was shut off, the sphere contracted slightly as it returned to its original temperature. This is evidenced by the slight acceleration also shown in figure 21.

5.3.4 Deposition of Silver onto the Sphere

Current was passed through the silver filament until the surrounding glass turned black. This meant that silver molecules must have been sublimated and must have at least hit the sphere. Figures 22 and

23 are microscope photographs of the plain and silvered steel spheres respectively. The magnification of these photographs is not large enough to show surface roughness. An examination of the surface would perhaps be possible with LEED or an electron microscope.

5.3.5 Gross Counting Errors

These were minimized by plotting rps versus time for each test undertaken and rejecting that part of any curve which was not continuous or hinted at an abnormal deceleration.

CHAPTER VI

SUMMARY AND CONCLUSIONS

The following table summarizes the experimental data collected in this project. A detailed tabulation appears in tables 1 to 7 and the various measurements of σ are plotted versus absolute pressure in figures 18, 19 and 20.

Gas	Average σ Fresh Silver	Average σ Aged Silver
N_2	.93	.93
A	.95*	.91
He	.43	.89

* Inaccurately measured

In a preliminary test with N_2 on plain polished steel, the average value of σ was found to be .88.

These measurements confirm that the reflection process on a relatively clean surface is not 100% diffuse. Other implications plus the effect of surface condition and contamination are discussed more fully in Chapter V.

The ionization gauge was the major source of experimental error. With an improved pressure gauge, plus the recommended equipment changes, the tangential accommodation on a moving surface could be very accurately measured. While this method does not give direct information on the velocity distribution of reflected molecules, the accurate reliable values of σ are valuable for comparison with results of new

surface interaction theories as well as for the obvious direct engineering application. This apparatus is also useful for studying the effect on tangential accommodation of possible surface treatments such as the deposition of a film of silver as was used in the present investigation.

RECOMMENDED EQUIPMENT CHANGES

1. The ion gauge was a source of error and contamination. It should be replaced - preferably with a diaphragm type absolute pressure gauge. This diaphragm gauge would eliminate contamination and accurately measure total pressure regardless of the type or composition of gas. If equipped with a pressure readout, it would offer a permanent record of the chamber pressure throughout the complete test.
2. The container walls require better temperature regulation. A constant wall temperature could easily be maintained with a water-jacket adaptation or by enclosing the vacuum system in an oven. This would assure Maxwellian Velocity Distribution of the molecules impinging on the sphere.
3. The system should be redesigned to include a means of gas analysis which would enable a study of the contaminants in the system thus assessing the effectiveness of the nickel getter. Perhaps another nickel getter in the same container as the sphere would be warranted.
4. The method used to raise the sphere into position requires modification. The present glass fixture was raised with a strong external magnet which could easily magnetize the sphere and increase its residual drag. A mechanical type feedthrough would seem to be the most obvious replacement of this fixture.
5. Perhaps the driving coils, magnetic shielding etc., could be improved so that the residual drag would be reduced to a level low enough to be neglected entirely. Beams (9) constructed a similar

magnetic suspension system which has a residual drag equivalent to a gas pressure of 10^{-9} torr.

6. The counting system could be modified using a stronger light source and different photodiode setup. This would enable operation at higher RPM's, perhaps with peripheral speeds as high as the mean free velocity of the gas molecules.
7. A DC power supply with a finer current adjustment would enable a better control of the evaporation rate from the silver and nickel filaments. These filaments should also be redesigned to allow replacement when burnt out.
8. It would be advantageous to isolate the apparatus more effectively from building vibrations.
9. The roughing pump should be analyzed to ascertain if a lower and more desirable bakeout pressure could be maintained.
10. The system would be improved by a design such that the calibration sphere (if used) could be inserted into the magnetic suspension system without venting the chamber to atmospheric pressure.

LITERATURE CITED

1. W.J. Schaetzle, "Some Experimental Data on Momentum Accommodation Factors", Rarefied Gas Dynamics, Proc. 5th Int. Sym. on Rarefied Gas Dynamics (1966), Volume 1, 1967, pp. 211-222.
2. J.N. Smith, Jr. and H. Saltzburg, "Recent Studies of Molecular Beam Scattering from Continuously Deposited Gold Films", Rarefied Gas Dynamics, Proc. 4th Int. Sym. on Rarefied Gas Dynamics (1964), Volume II, 1966, p. 491.
3. H. Saltzburg, J.N. Smith, Jr., and R.L. Palmer, "Scattering of Molecular Beams of He, D_2 and H_2 from the (111) Plane of Ag", Rarefied Gas Dynamics, Proc. 5th Int. Sym. on Rarefied Gas Dynamics (1966), Volume I, 1967, pp. 223-252.
4. Sir J. Jeans, "An Introduction to the Kinetic Theory of Gases", Cambridge University Press, 1940, p. 2.
5. E.H. Kennard, "Kinetic Theory of Gases", McGraw-Hill, 1938.
6. G.N. Patterson, "Mechanics of Rarefied Gases and Plasmas", UTIAS Review 18, 1964.
7. J.J. Hinchen and E.F. Shepard, "Molecular Beam Scattering From Surfaces of Various Metals", Rarefied Gas Dynamics, Proc. 5th Int. Sym. on Rarefied Gas Dynamics (1966), Volume I, 1967, pp. 239-252.
8. C. Chree, "The Stresses and Strains in Isotropic Elastic Solid Ellipsoids derivable from a Potential of the Second Degree", Proc. Roy. Soc. of London, Volume 58, 1895, pp. 39-59.

9. J.W. Beams, "Double Magnetic Suspension", Rev. Sci. Inst., Volume 34, 1963, pp. 1071-1074.

10. J.W. Beams, J.L. Young and J.W. Moore, "The Production of High Centrifugal Fields", J. Appl. Phys., Volume 17, 1946, p. 886.

11. S. Dushman, "Scientific Foundations of Vacuum Technique", Wiley, 1962, pp. 254, 256.

12. B.M.W. Trapnell, "The Activities of Evaporated Metal Films in Gas Chemisorbtion", Proc. Roy. Soc. of London, Volume A218, 1952, p. 566.

13. F.C. Hurlbut, "Current Developments in the Study of Gas-Surface Interactions", Rarefied Gas Dynamics, Proc. 5th Int. Sym. on Rarefied Gas Dynamics (1966), Volume I, 1967, pp. 1-34.

14. G. Lewin, "Fundamentals of Vacuum Science and Technology", McGraw-Hill, 1965, pp. 147-148.

15. H.Y. Wachman, "Accommodation Coefficients of Nitrogen and Helium on Nitrogen Covered Tungsten Between 325-496 Degrees K", Rarefied Gas Dynamics, Proc. 5th Int. Sym. on Rarefied Gas Dynamics (1966), Volume I, 1967, pp. 173-186.

16. N. Abuaf and D.G.H. Marsden, "Momentum Accommodation of Argon in the 0.06 to 5 ev Range", Rarefied Gas Dynamics, Proc. 5th Int. Sym. on Rarefied Gas Dynamics (1966), Volume I, 1967, pp. 199-210.

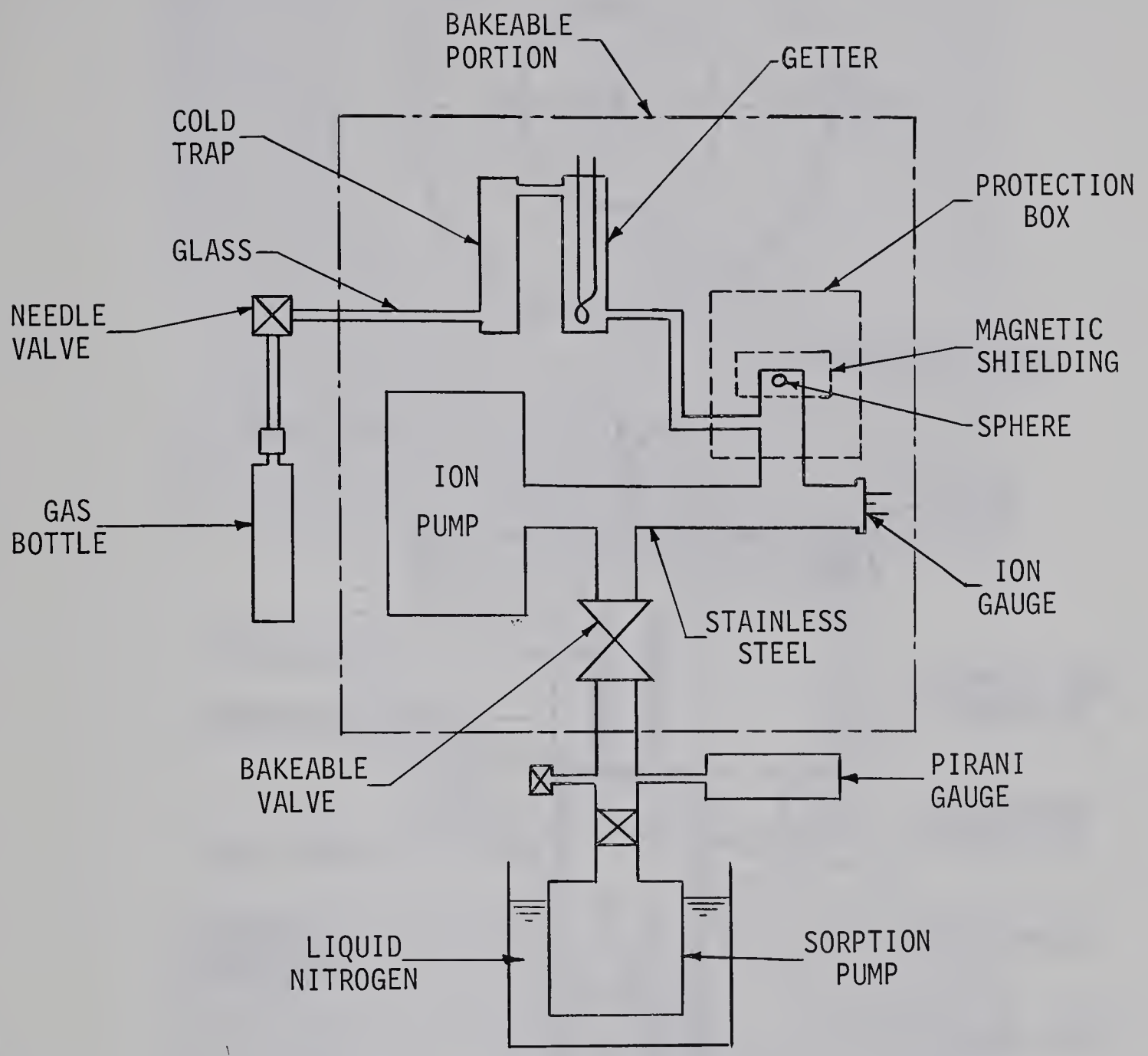

Figure 1. SCHEMATIC DIAGRAM OF EXPERIMENTAL APPARATUS

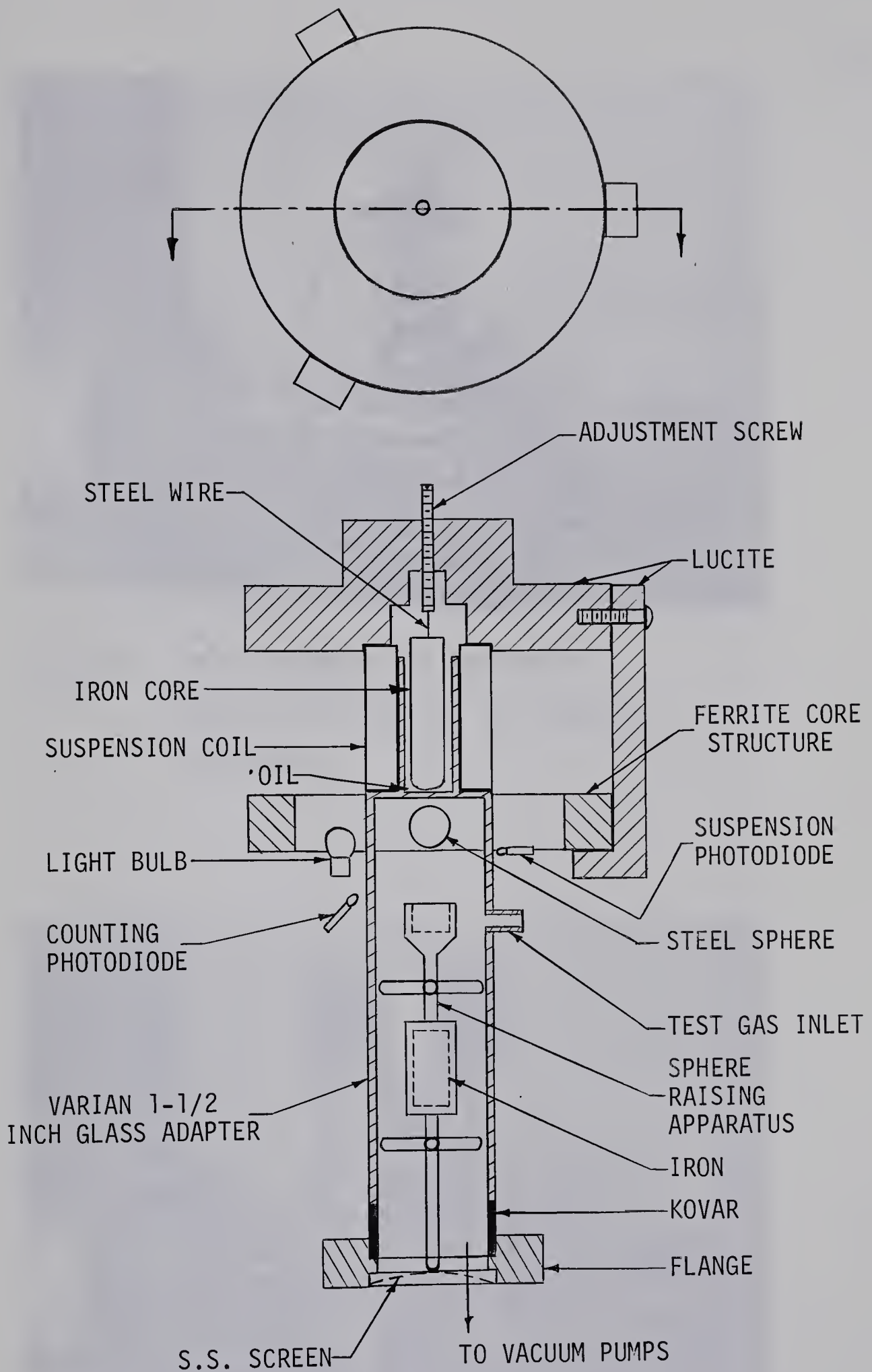

Figure 2. GENERAL ASSEMBLY OF SPHERE VACUUM CHAMBER

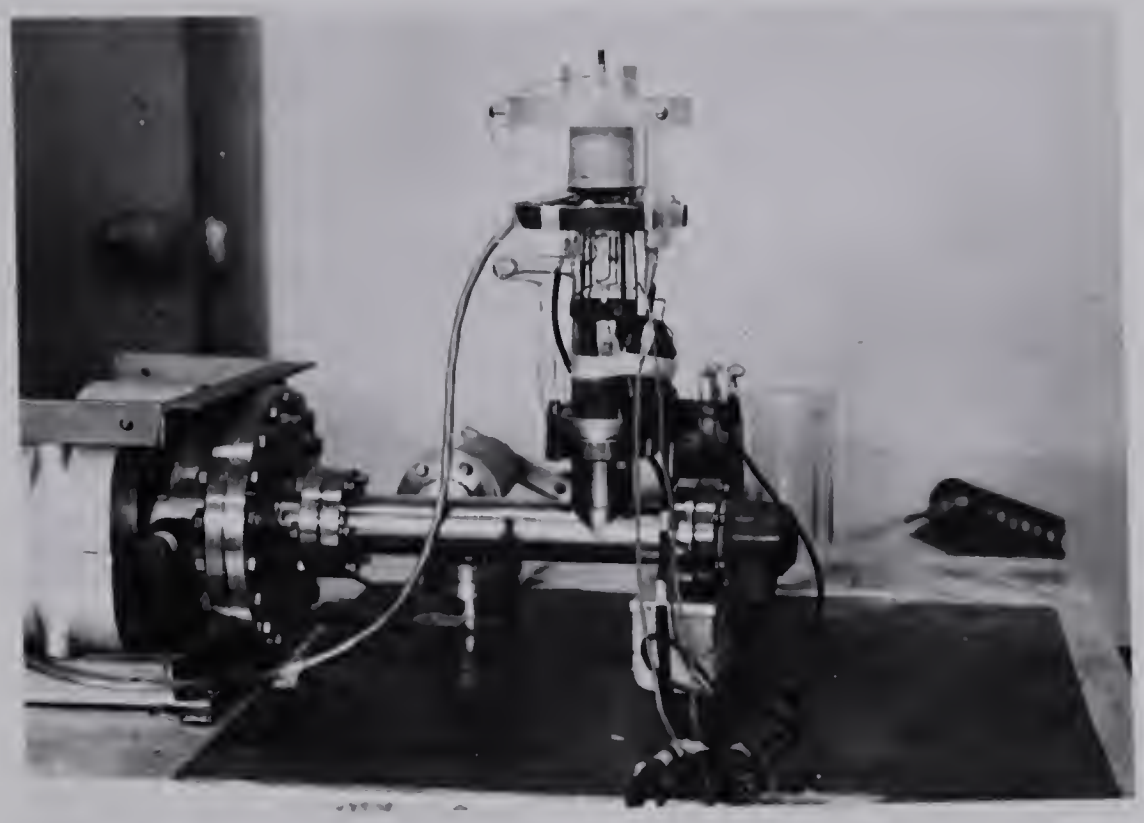

Figure 3 TEST CHAMBER AND ION PUMP WITH NO PROTECTIVE OR MAGNETIC SHIELDING

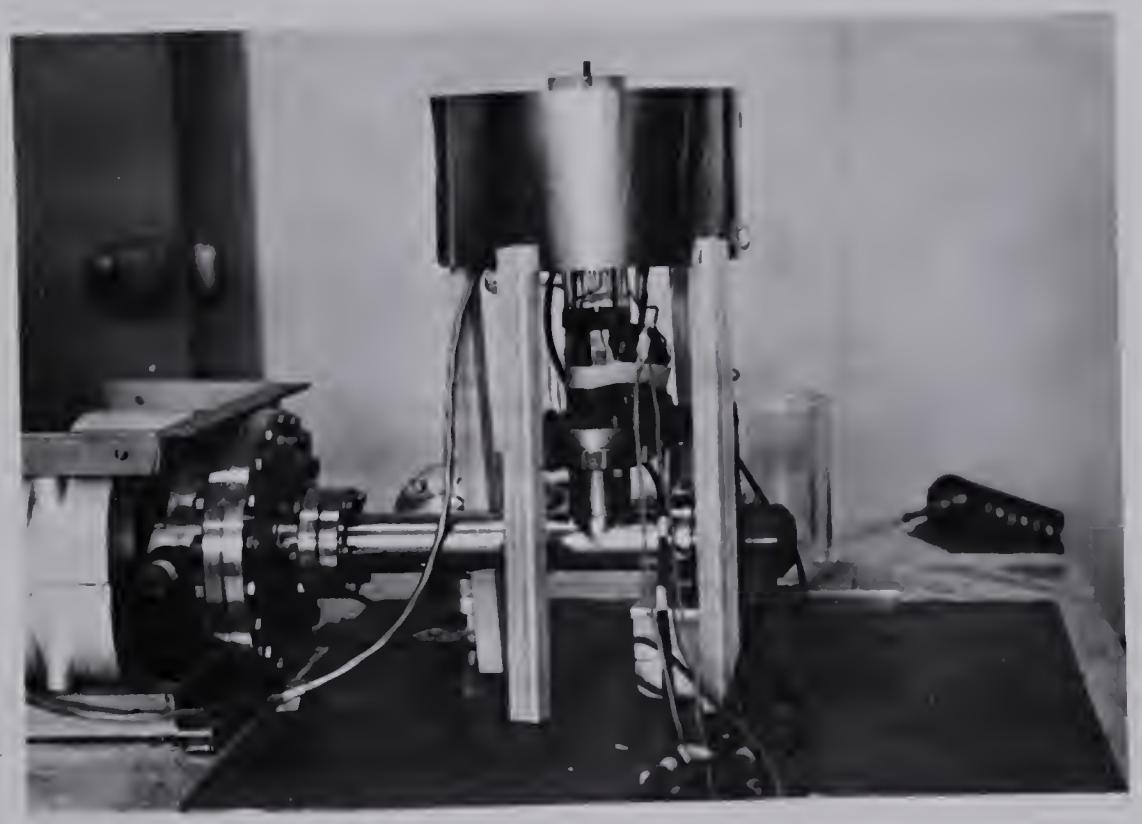

Figure 4 APPARATUS WITH CONETIC MAGNETIC SHIELDING

Figure 5 APPARATUS WITH MILD STEEL PROTECTION BOX

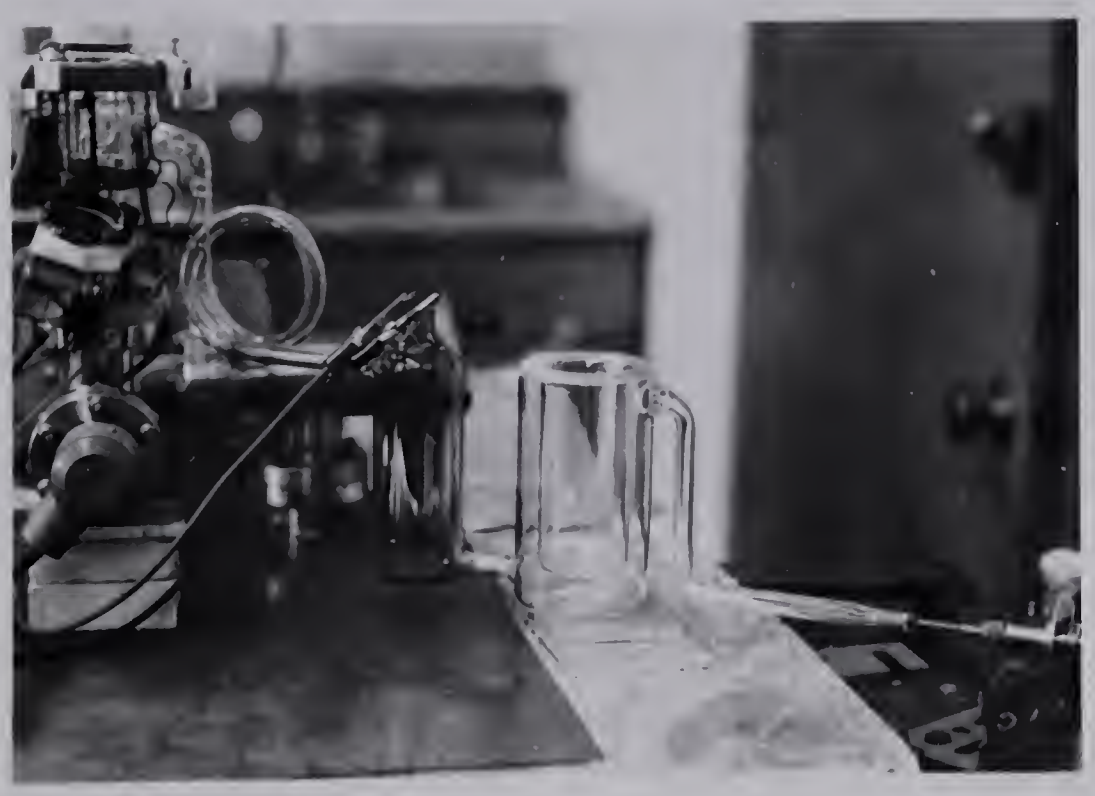

Figure 6 GLASS INLET LINE WITH NICKEL SELECTIVE GETTER AND COLD TRAP

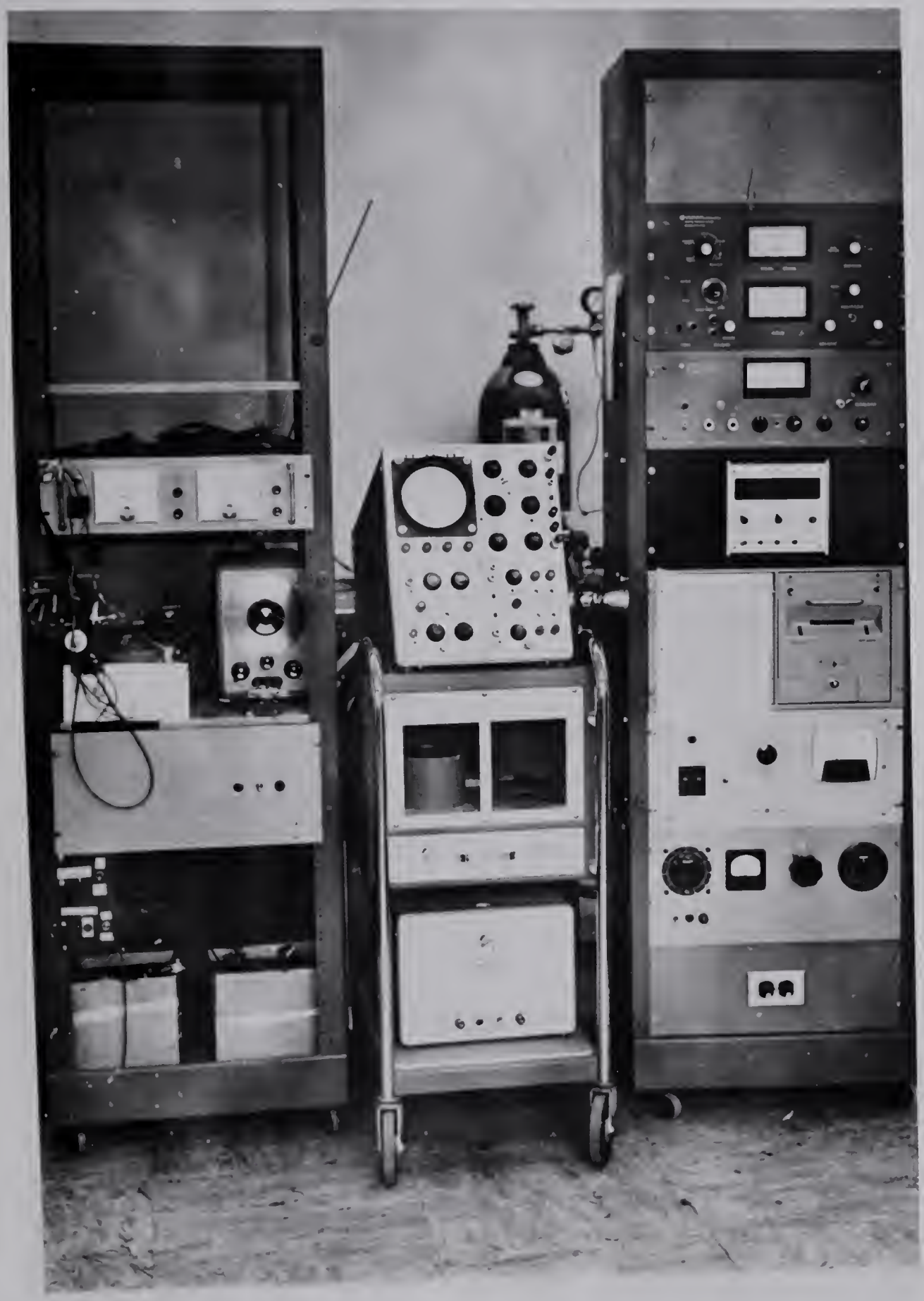

Figure 7 INSTRUMENT PANEL

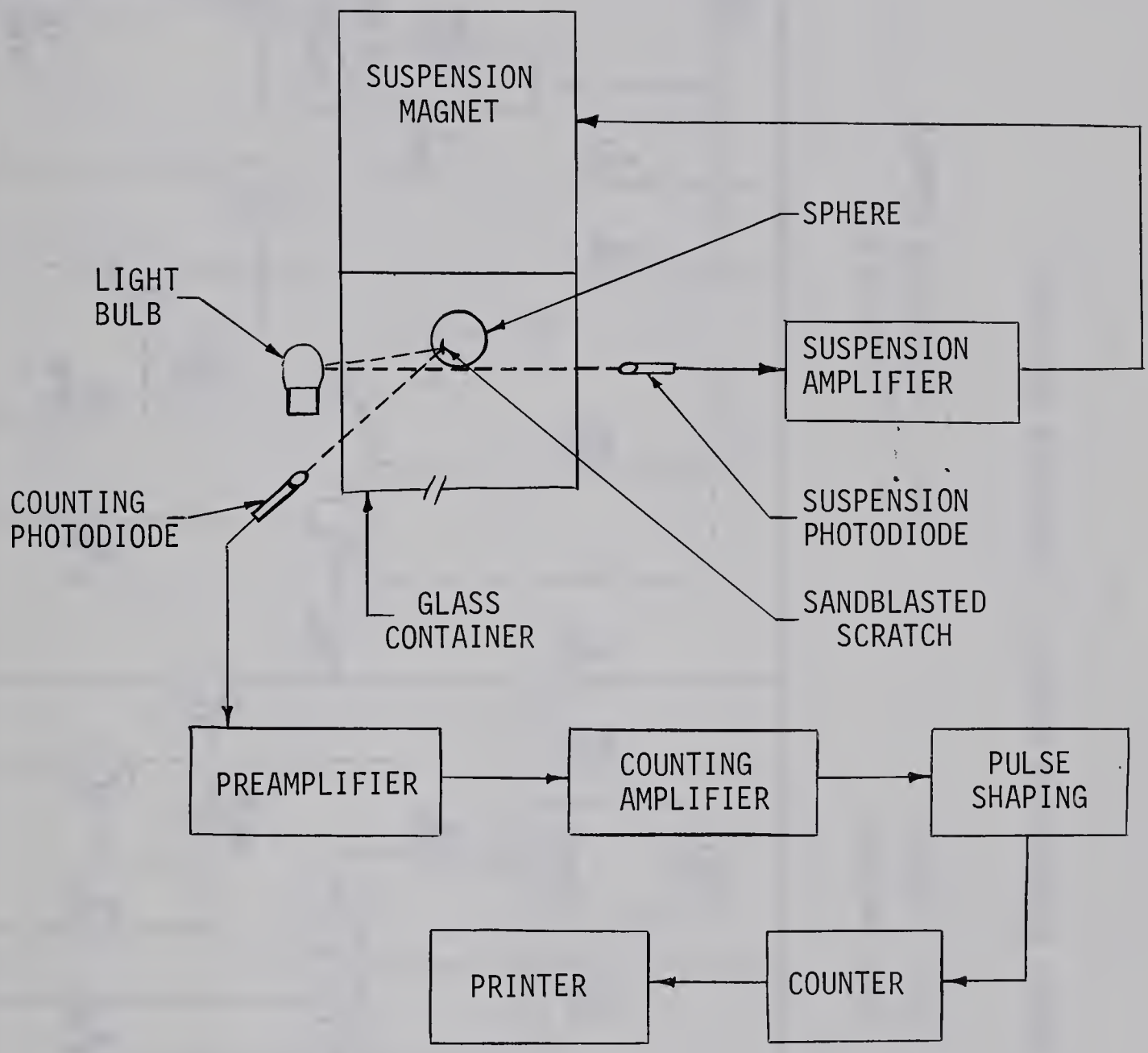

Figure 8. BLOCK DIAGRAM OF SUSPENSION AND COUNTING SYSTEM

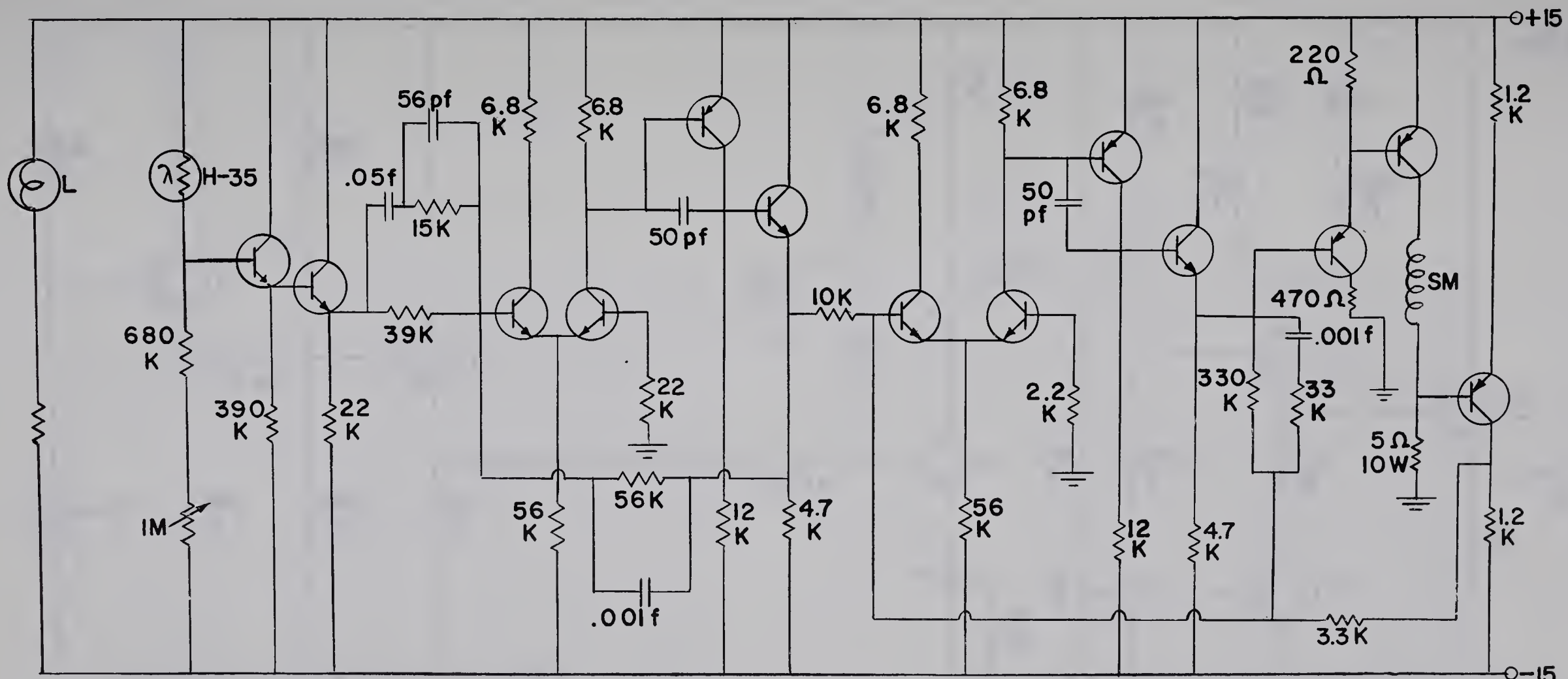

TRANSISTORS PNP - 2N3702

NPN - 2N3707

L = LIGHT BULB

SM = SUSPENSION MAGNET

Figure 8a. CIRCUIT DIAGRAM FOR MAGNETIC SUSPENSION AMPLIFIER

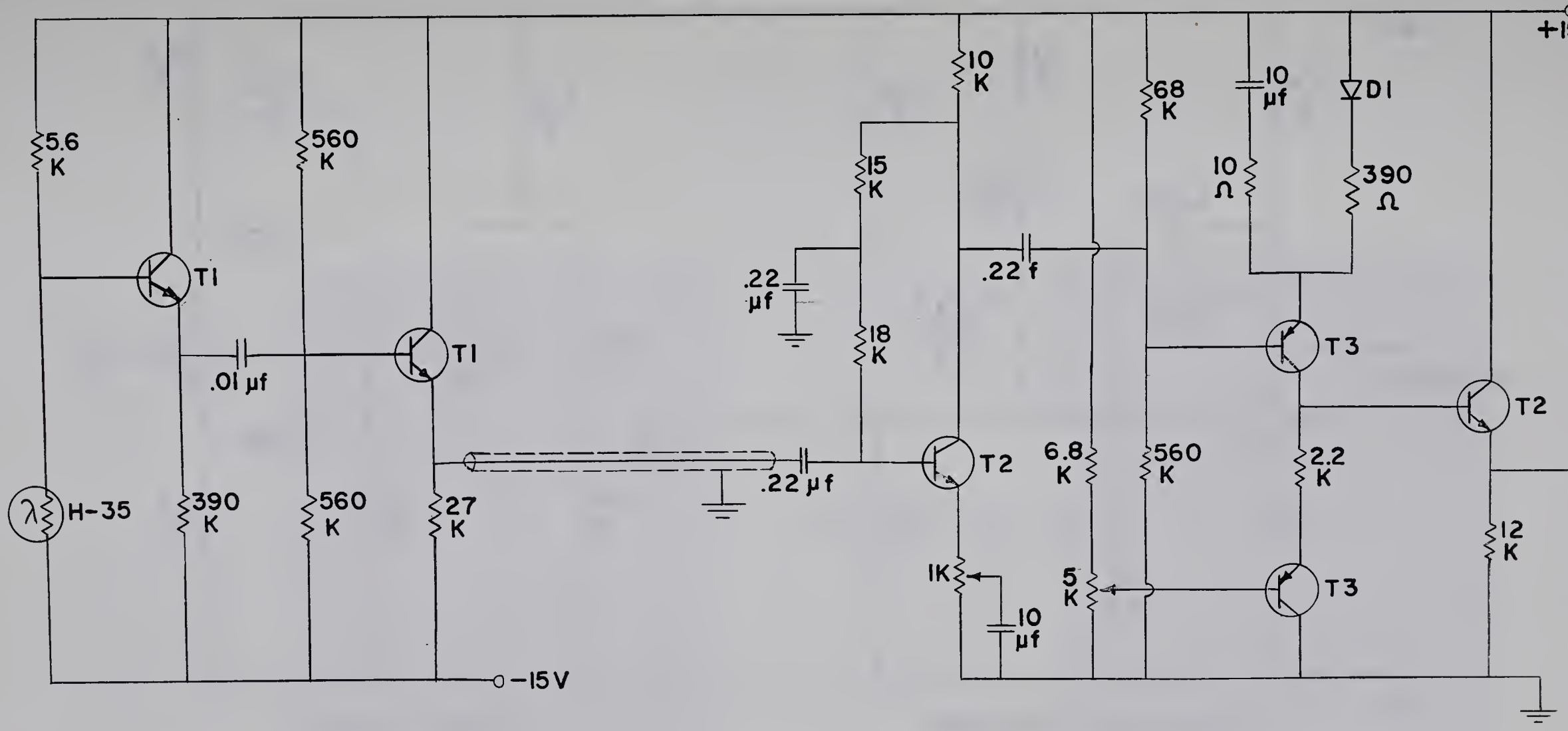

PREAMPLIFIER

AMPLIFIER AND LEVEL SHIFTER

T1 = 2N3707 T3 = 2N3702 A - TO SCHMITT TRIGGER

T2 = 2N3704 D1 = 1N456

Figure 8b. CIRCUIT DIAGRAM FOR PREAMPLIFIER AND AMPLIFIER - COUNTING SYSTEM

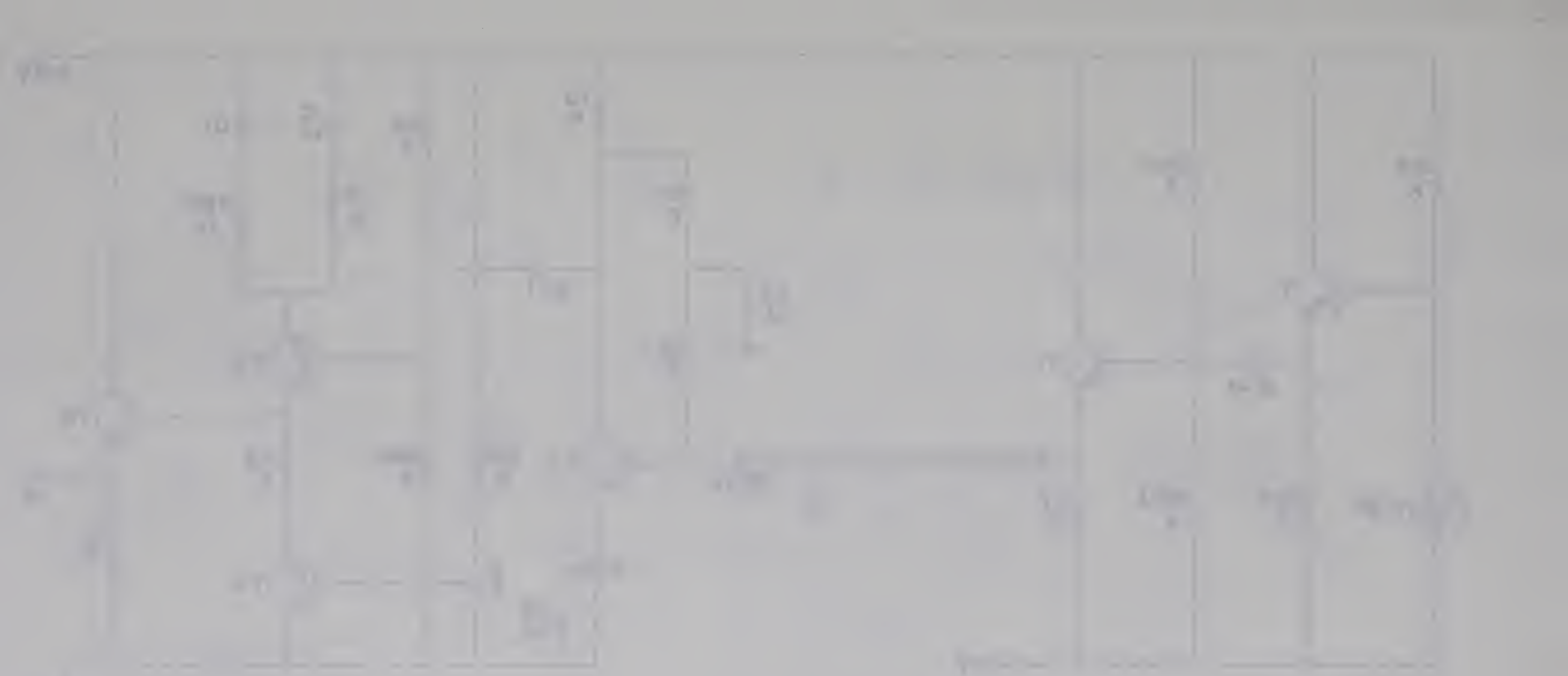

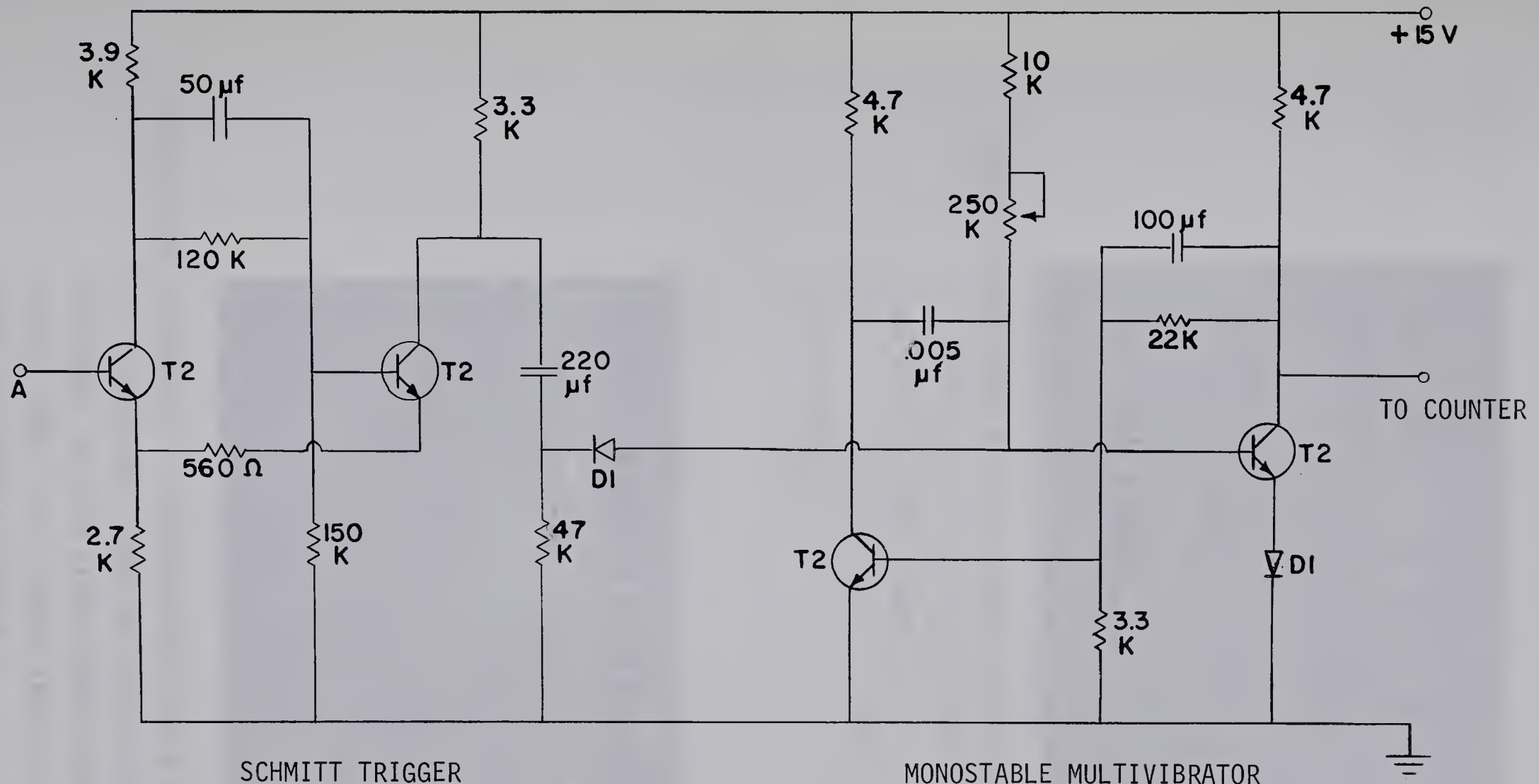

T2 = 2N3704 A - FROM AMPLIFIER

D1 = 1N456

Figure 8c. CIRCUIT DIAGRAM FOR PULSE SHAPING CIRCUIT - COUNTING SYSTEM

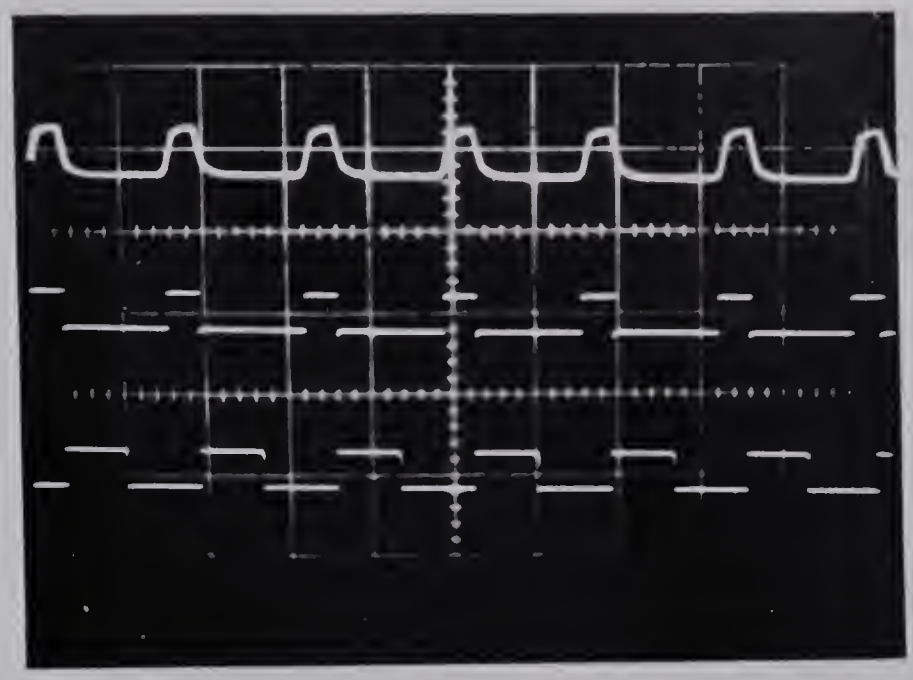

Figure 9 PHOTOGRAPH OF OSCILLOSCOPE SCREEN SHOWING THE PHOTODIODE SIGNAL AT LOW RPM'S ON THE TOP TRACE AND THE FINAL SHAPED SIGNAL ON THE BOTTOM TRACE. THE MIDDLE TRACE IS TAPPED FROM THE SCHMITT TRIGGER.

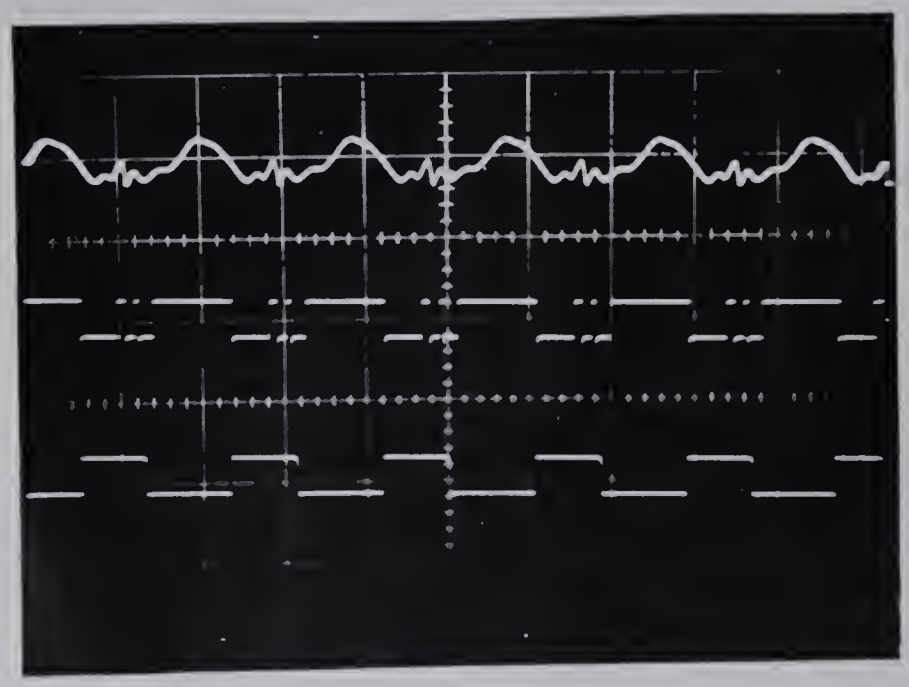

Figure 9a PHOTOGRAPH OF OSCILLOSCOPE SCREEN SHOWING THE PHOTODIODE SIGNAL AT HIGHER RPM'S ON THE TOP TRACE AND THE FINAL SHAPED SIGNAL ON THE BOTTOM TRACE. THE MIDDLE TRACE IS TAPPED FROM THE SCHMITT TRIGGER.

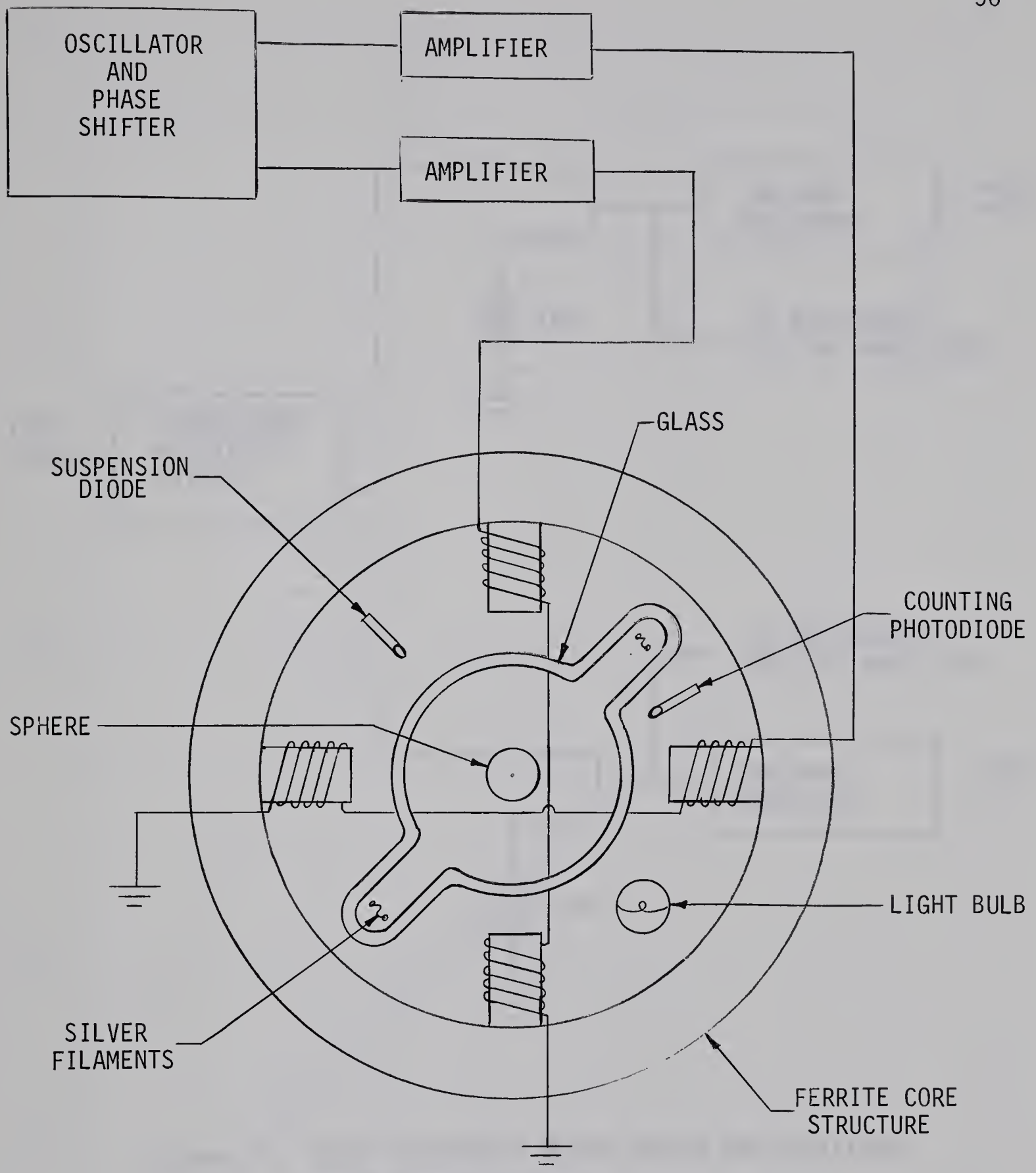

Figure 10. SCHEMATIC OF ROTATIONAL DRIVING SYSTEM

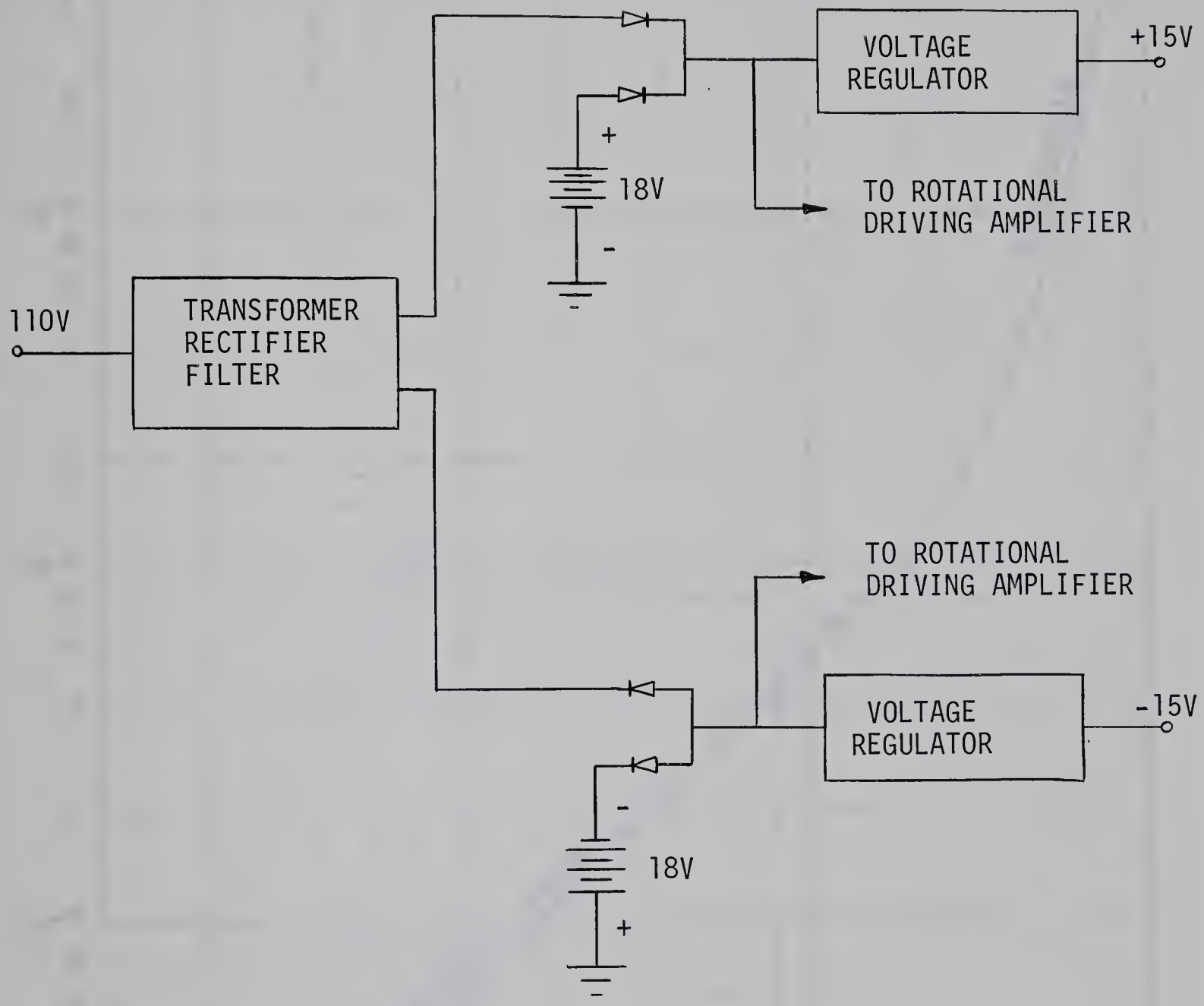

Figure 11. BLOCK DIAGRAM OF POWER SUPPLY AND AUXILIARY POWER SUPPLY SYSTEMS

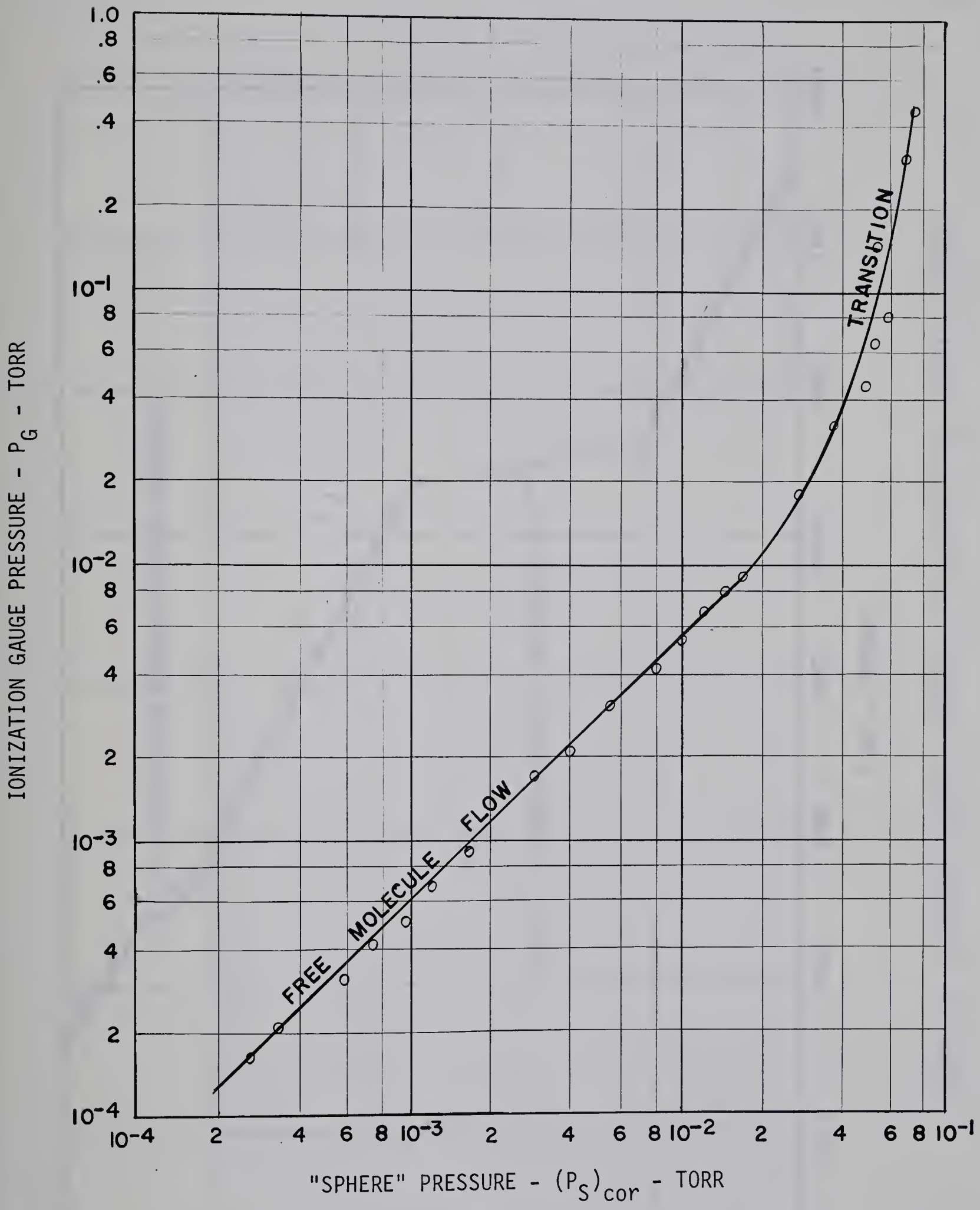

Figure 12. CALIBRATION WITH OXIDIZED SPHERE

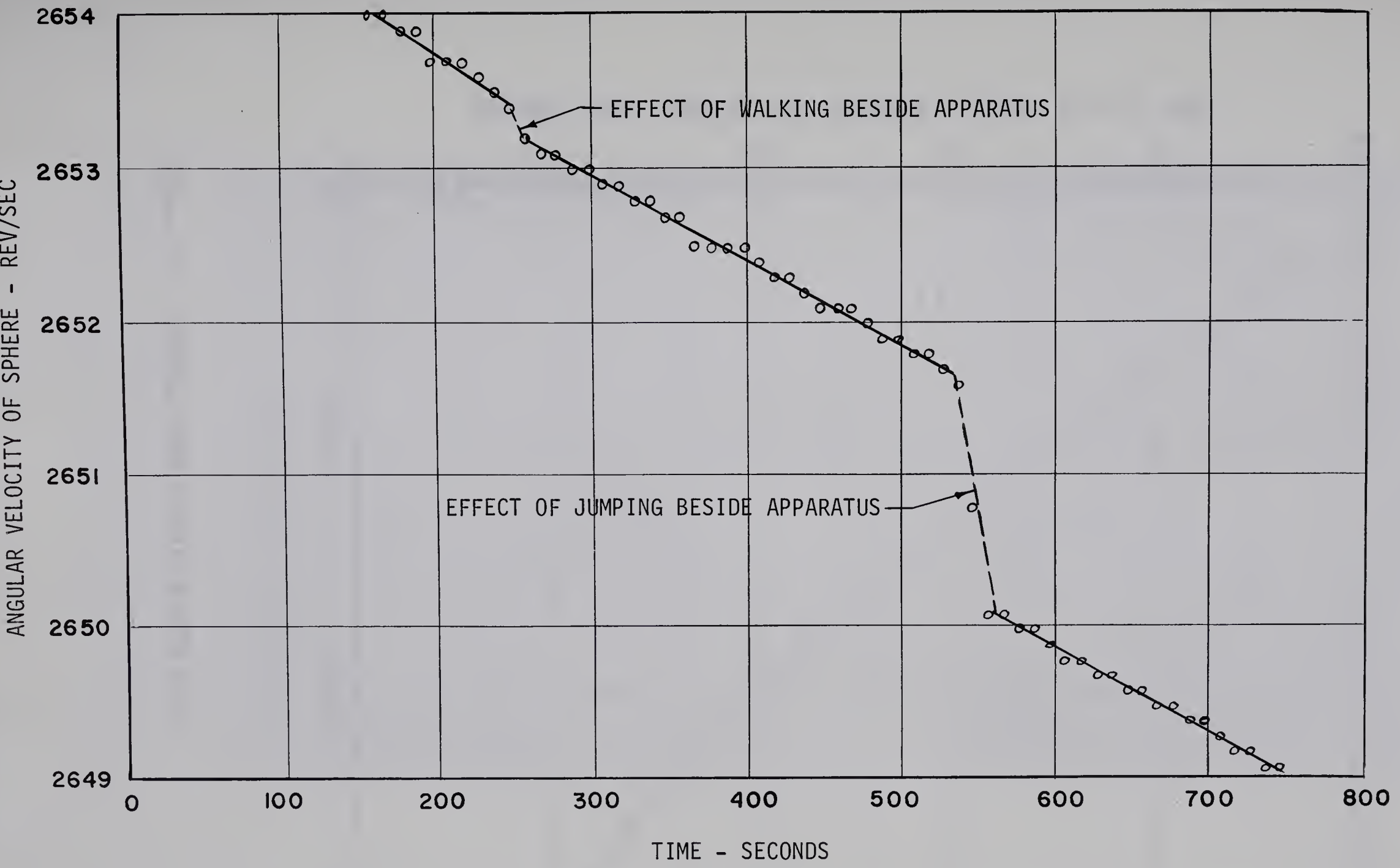

Figure 13. BUILDING MOVEMENT EFFECTS ON DECELERATION OF COASTING SPHERE

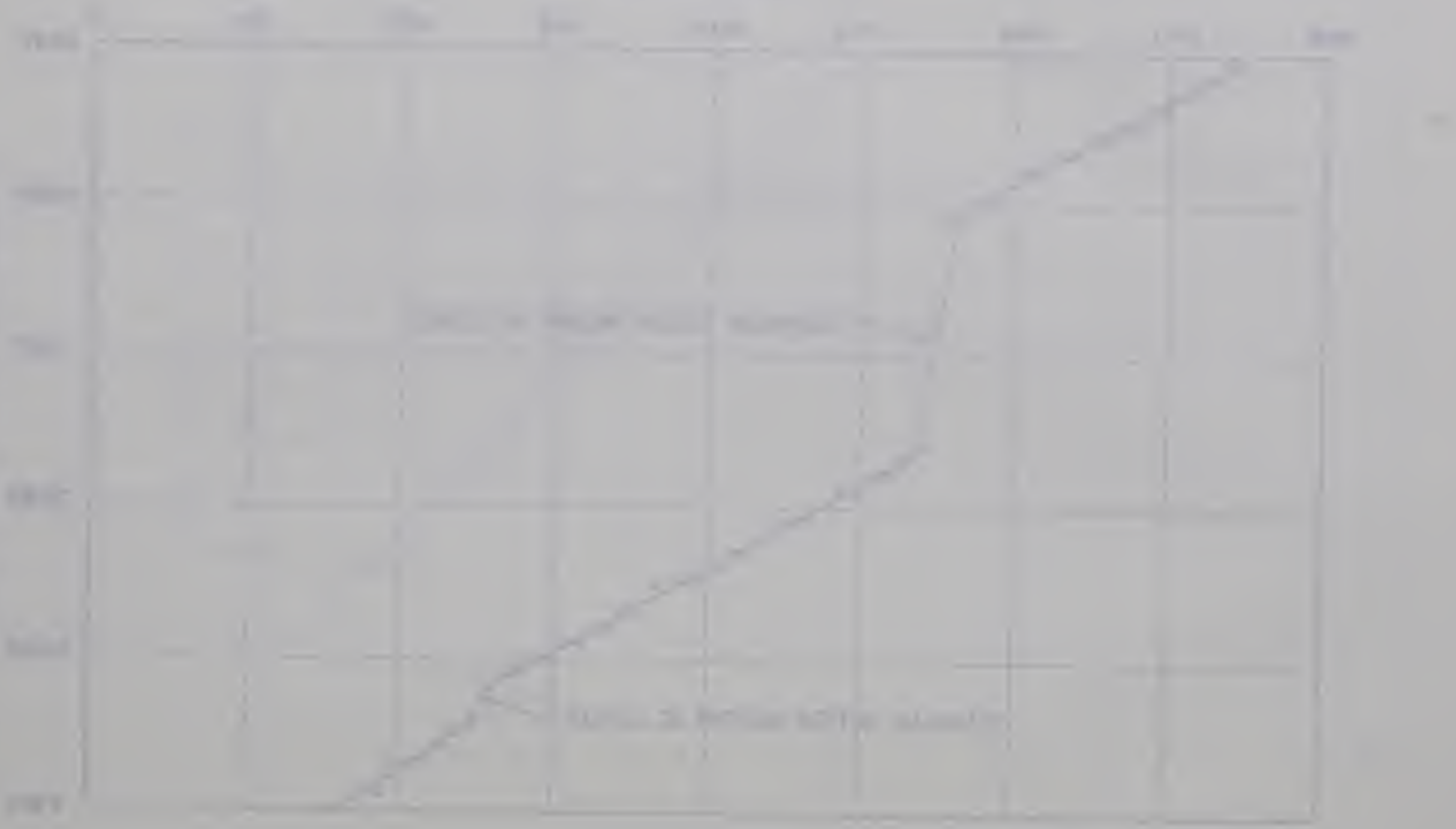

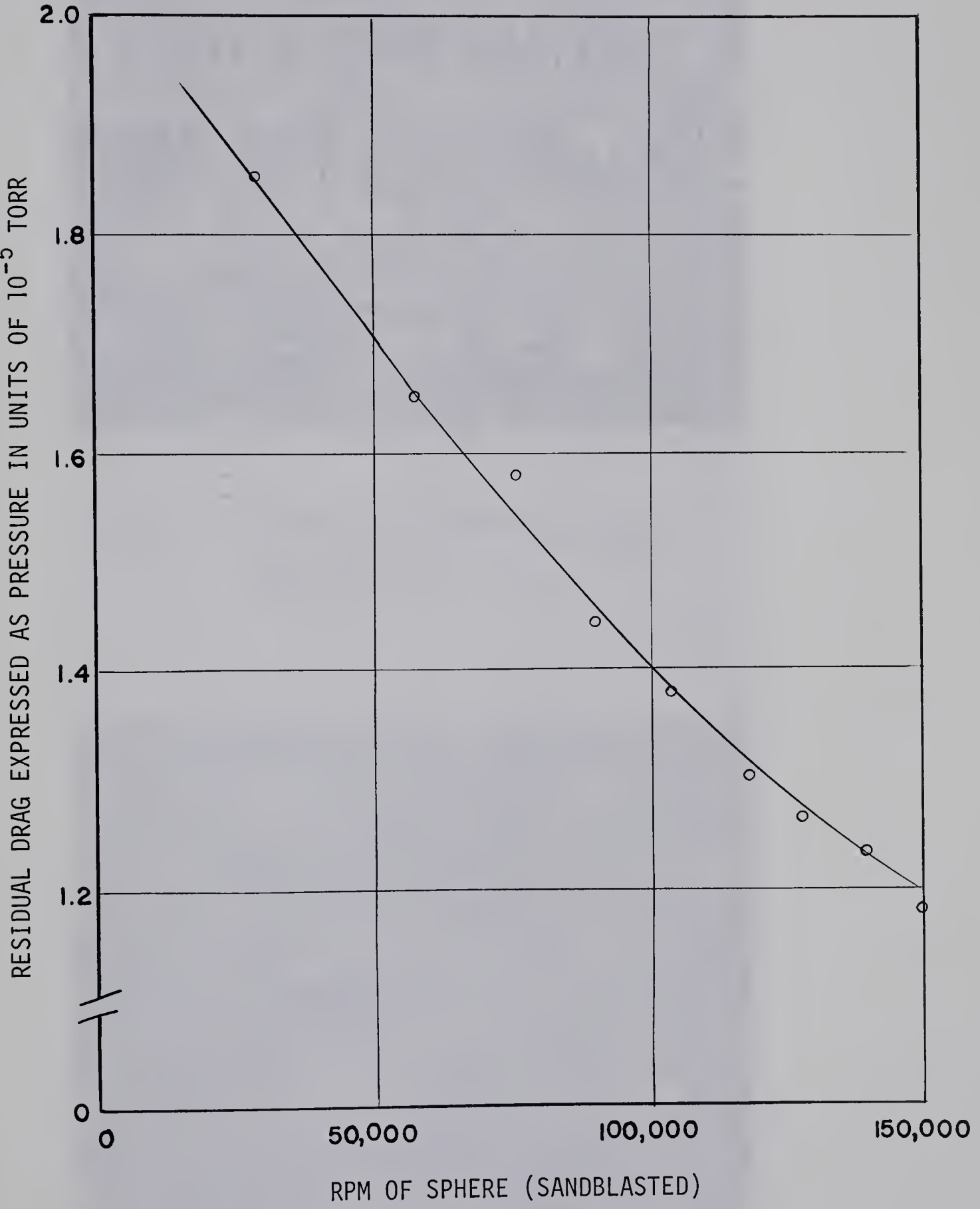

Figure 14. RESIDUAL DRAG VARIATION WITH RPM

Figure 15 OXIDIZED CALIBRATION SPHERE
MAGNIFICATION = 500x

Figure 16 SANDBLASTED CALIBRATION SPHERE
MAGNIFICATION = 500x

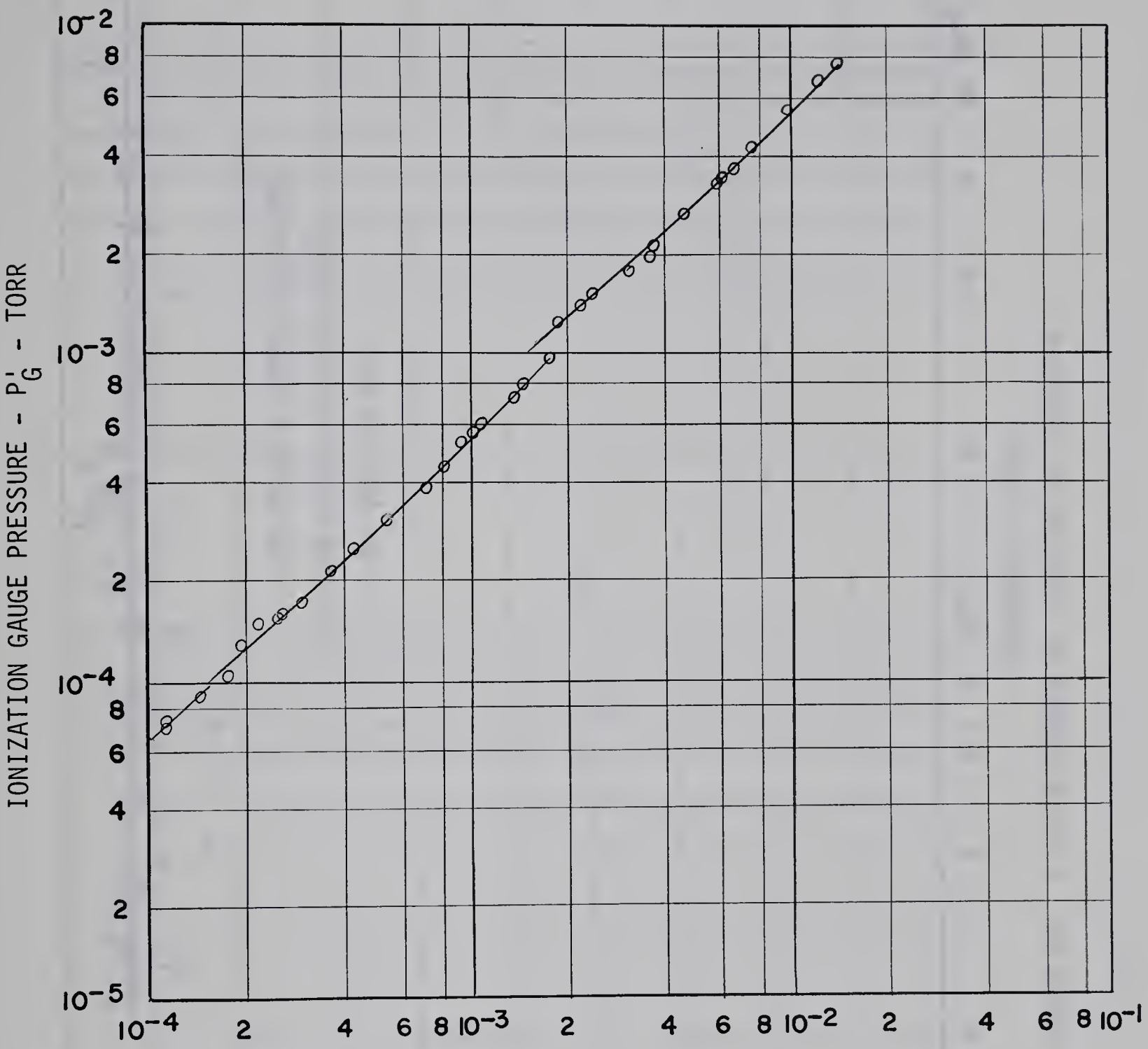

Figure 17. CALIBRATION CURVE FOR NITROGEN ON SANDBLASTED SPHERE

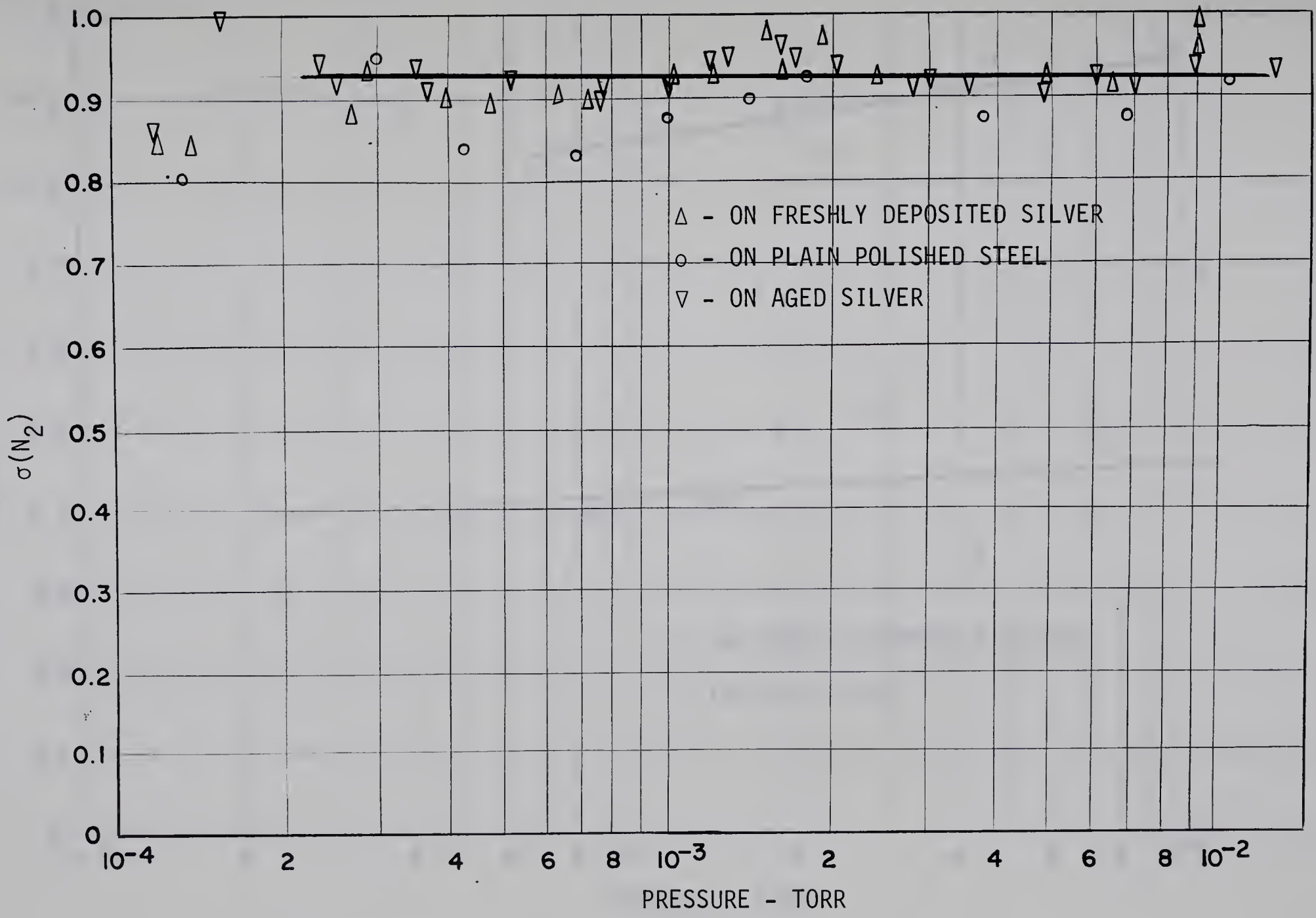

Figure 18. σ FOR NITROGEN AS FUNCTION OF PRESSURE

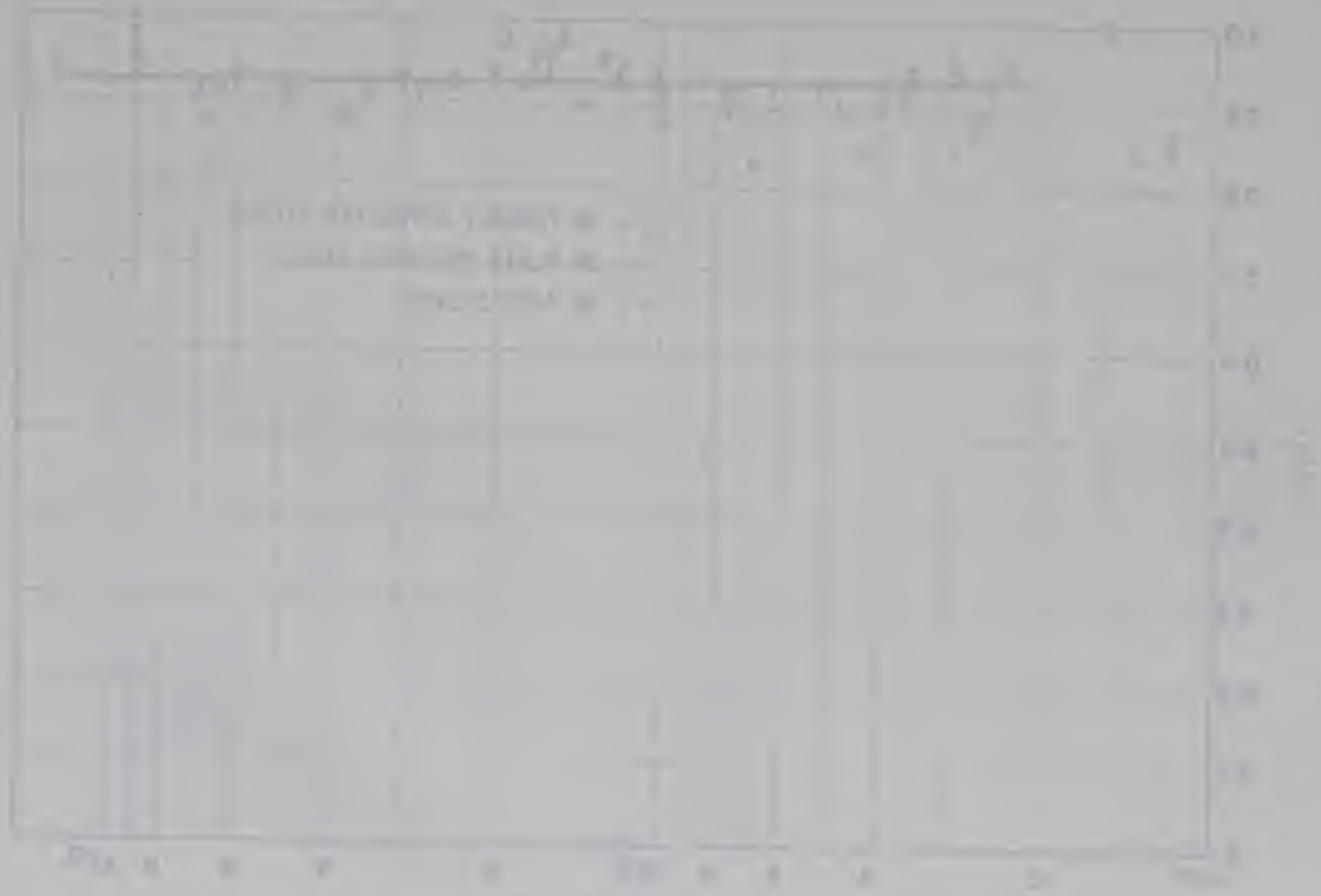

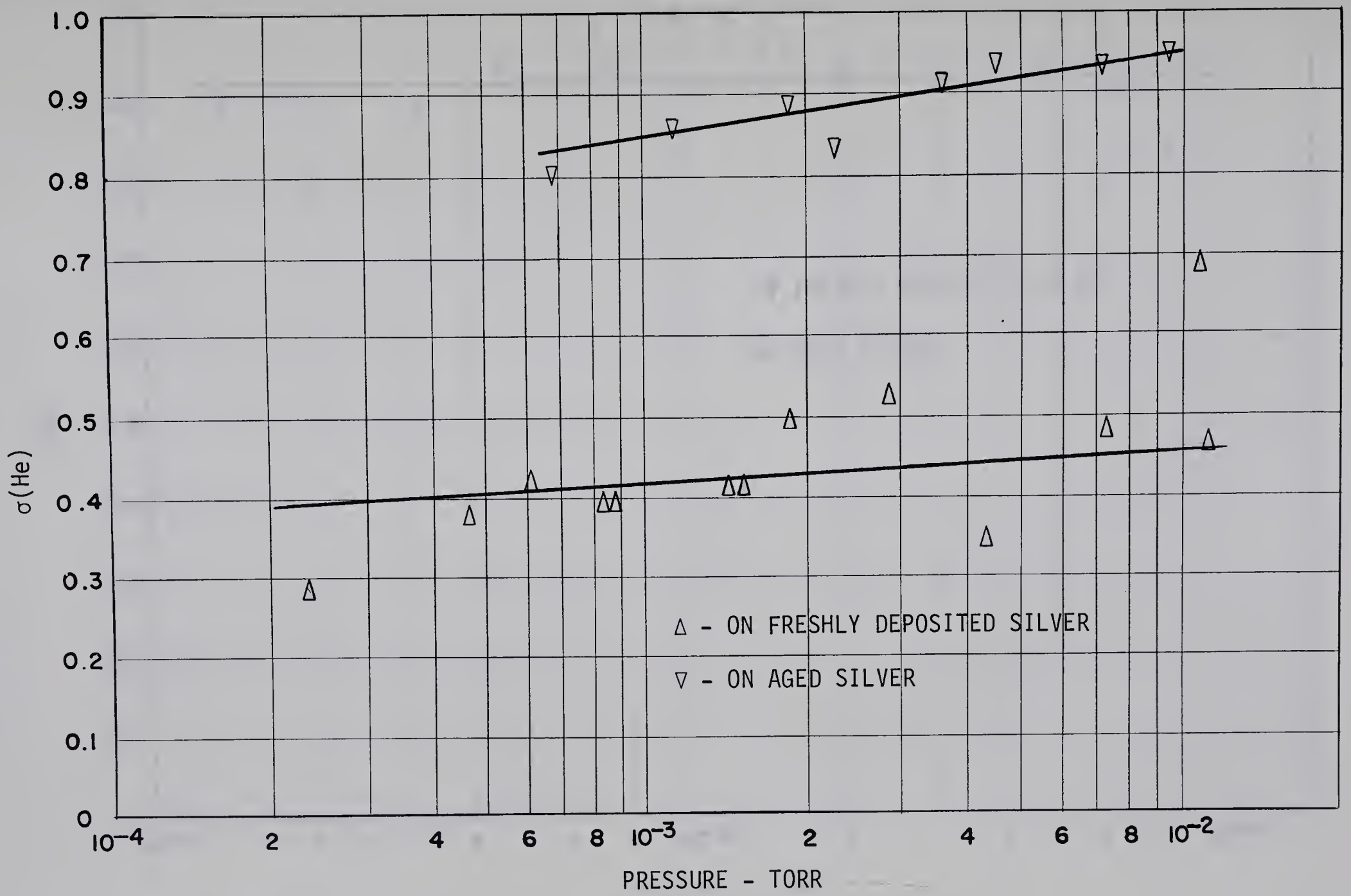

Figure 19. σ FOR HELIUM AS FUNCTION OF PRESSURE

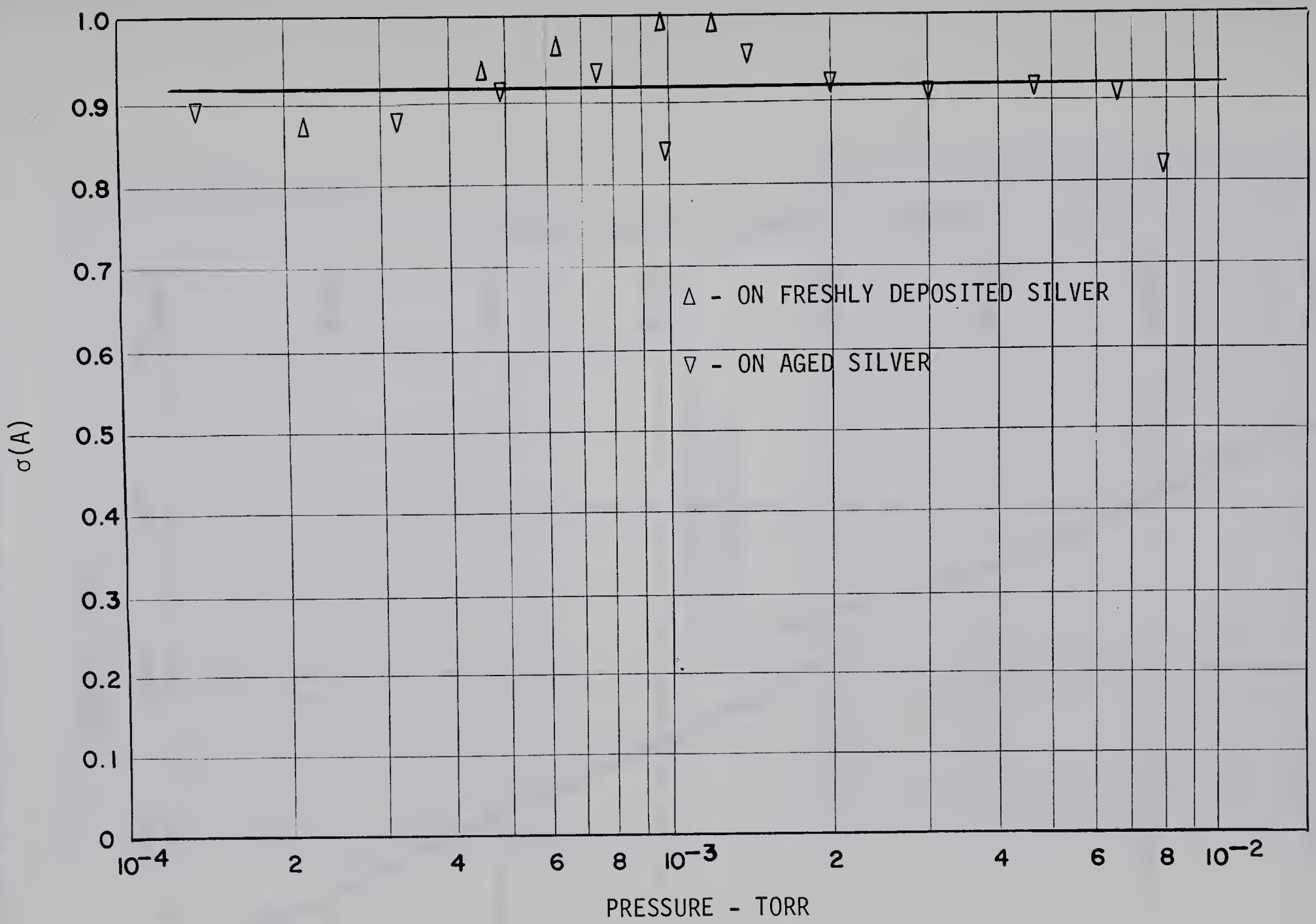

Figure 20. σ FOR ARGON AS FUNCTION OF PRESSURE

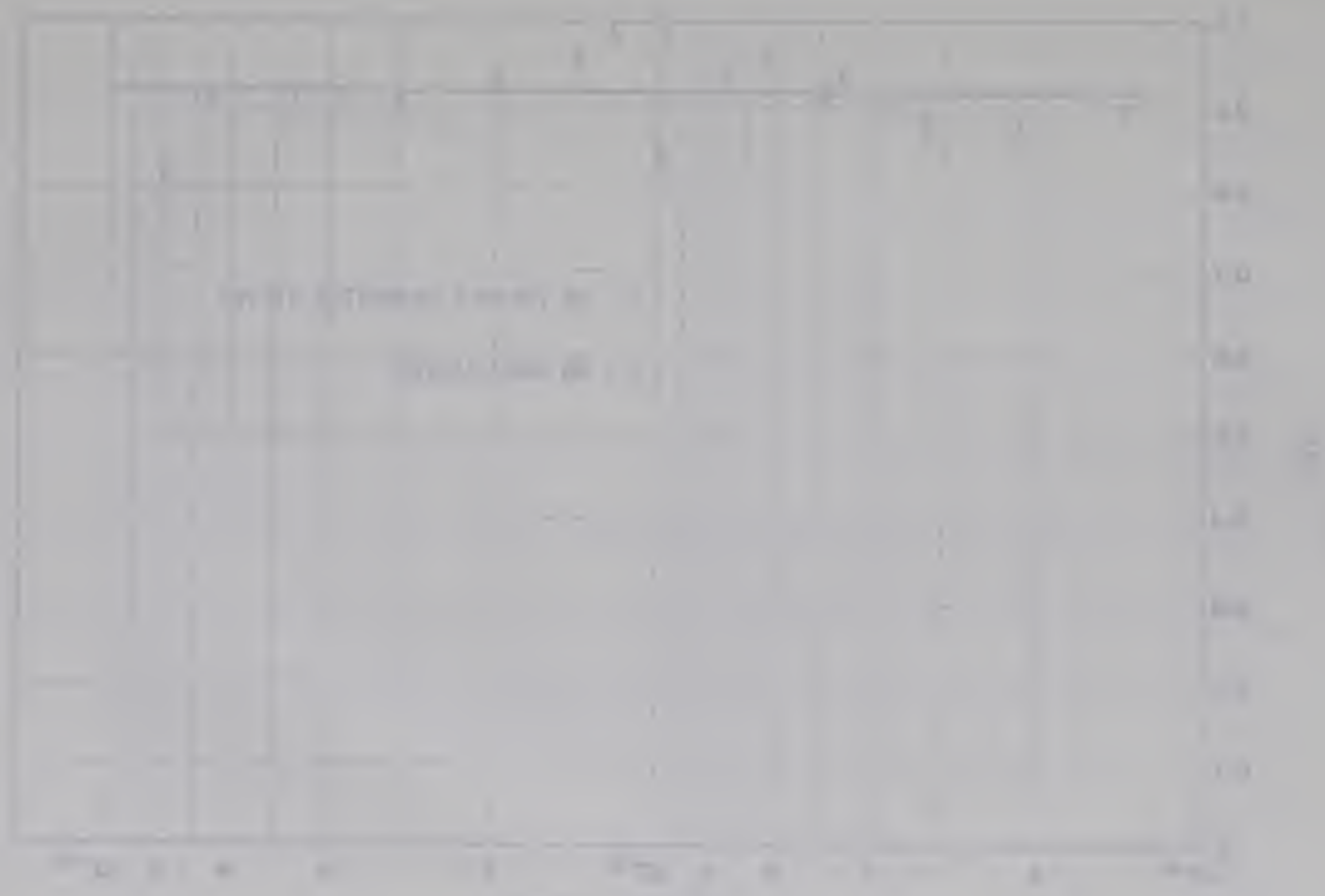

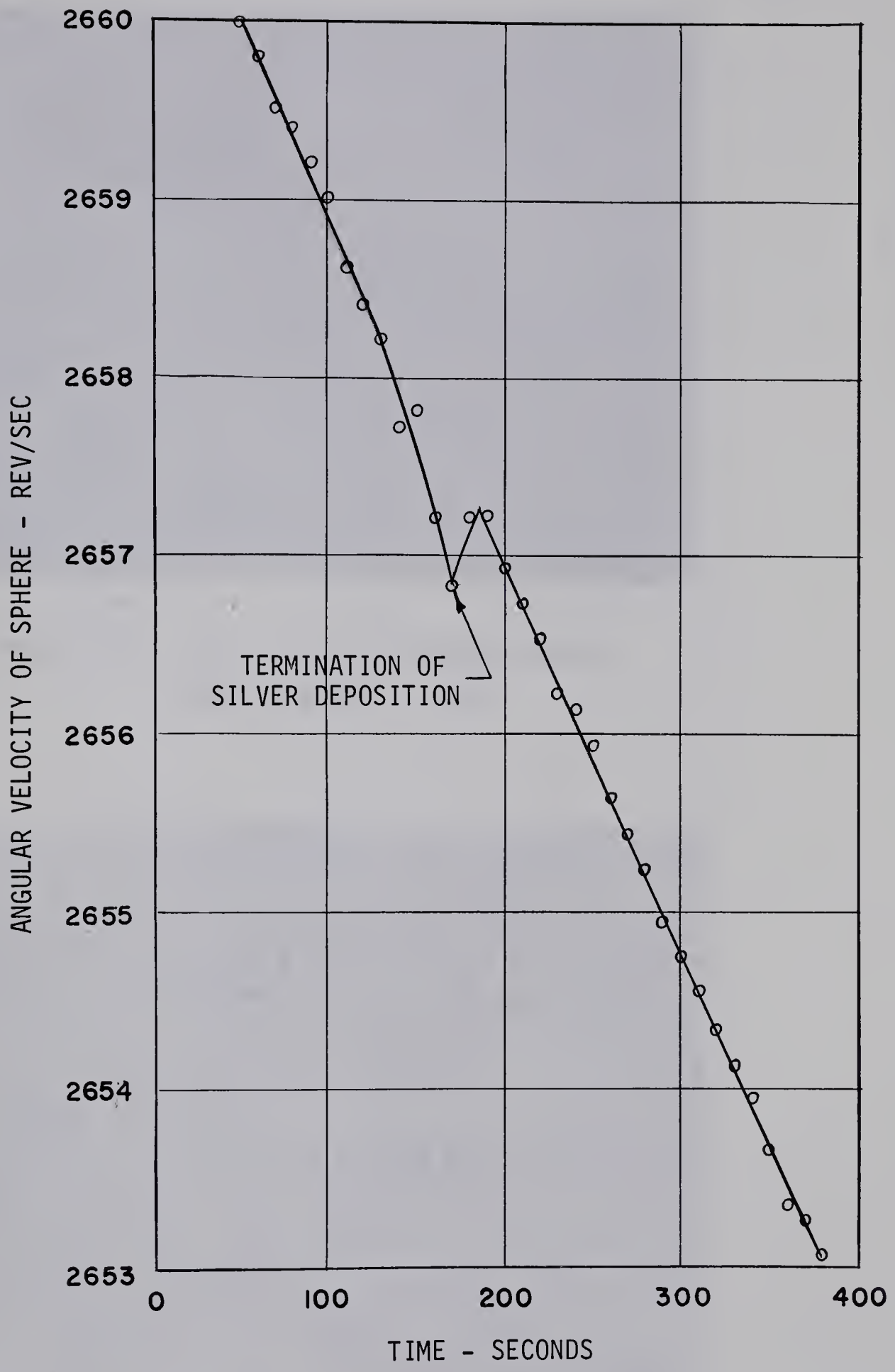

Figure 21 EFFECT OF SILVER DEPOSITION ON DECELERATION OF SPHERE AT LOW PRESSURE (1.75×10^{-4} TORR)

Figure 22 PLAIN POLISHED STEEL SPHERE
MAGNIFICATION = 500x

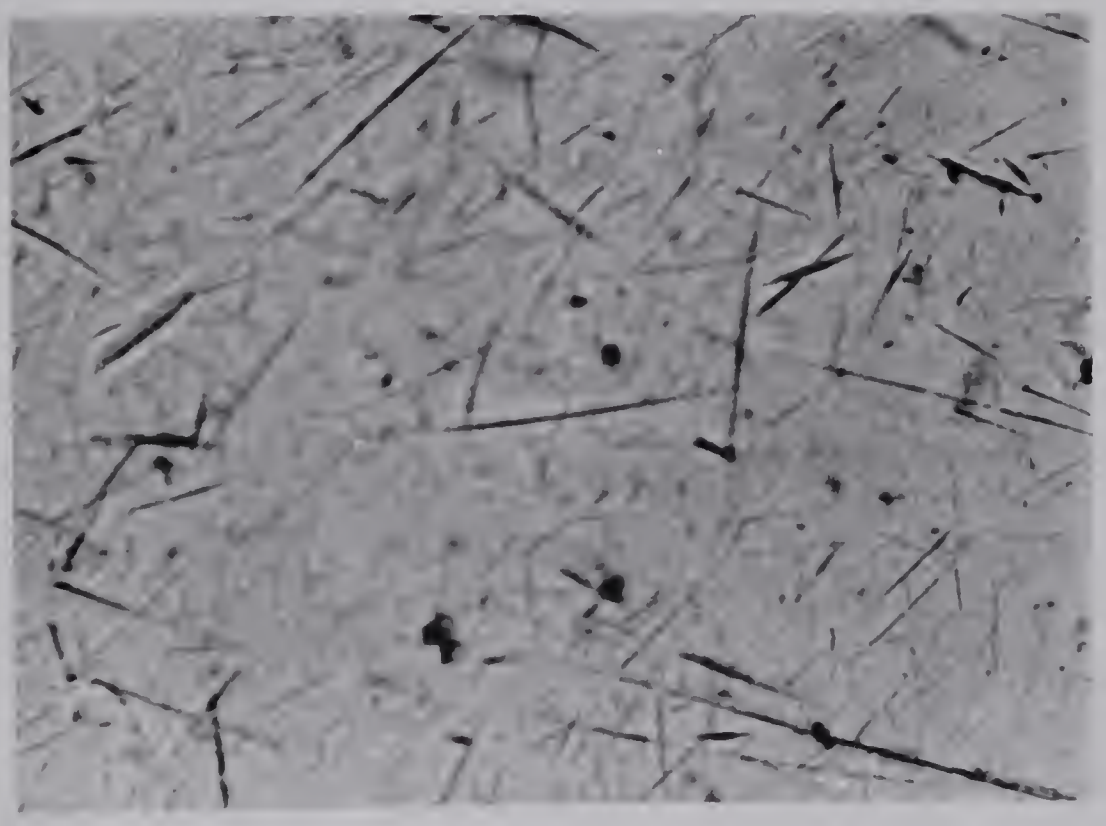

Figure 23 SPHERE AFTER DEPOSITION OF SILVER
MAGNIFICATION = 500x

TABLE 1

Experimental Data for N_2 on Plain Steel - July 17

Run No.	Time Sec.	Approx. RPM	P_G[2] Torr x 10^{-4}	$(P_S)_{cor}$ Torr x 10^{-4}	σ
A	660	84,000	P_{RD}[3] = 4.94 x 10^{-5}		
B	660	167,000	P_{RD} = 3.69 x 10^{-5}		
1	300	167,000	.85[1]	.75	.87
2	320	166,500	1.75	1.41	.81
3	250	166,000	3.30	3.14	.95
4	350	166,000	5.45	4.55	.84
5	430	165,000	8.50	7.15	.84
6	479	163,000	12.0[1]	10.5	.88
7	420	160,000	16.5	14.9	.90
8	400	157,000	20.0	18.6	.93
9	640	151,000	44.5	39.3	.88
10	420	140,000	81.0	72.0	.88
11	350	129,000	120.0	110.	.92
C	600	116,500	P_{RD} = 4.52 x 10^{-5}		

[1] - inaccurate range of ionization gauge.

[2] - all measurements of P_G were corrected with calibration curve.

[3] - P_{RD} is the pressure equivalent of residual drag in units of torr.

TABLE 2

Experimental Data for N_2 on Fresh Silver - July 18

Run No.	Time Sec.	Approx. RPM	P_G Torr x 10^{-4}	$(P_S)_{cor}$ Torr x 10^{-4}	σ
A	900	161,000	$P_{RD} = 5.14 \times 10^{-5}$		
1	190	160,000	.77[1]	.93	1.21
2	350	160,000	1.70	1.44	.85
3	420	159,000	3.15	2.95	.94
4	420	158,500	4.45	4.04	.91
5	400	157,500	7.20	6.54	.91
6	390	155,000	11.1[1]	10.3	.93
7	300	152,000	15.5	15.4	.99
8	190	149,000	19.5	19.1	.98
9	130	145,000	52.5	48.9	.93
10	200	139,000	97.0	94.4	.97
B	780	133,000	$P_{RD} = 6.11 \times 10^{-5}$		

TABLE 2a

Repeat - N_2 on Fresh Silver - July 19

Run No.	Time Sec.	Approx. RPM	P_G Torr x 10^{-4}	$(P_S)_{cor}$ Torr x 10^{-4}	σ
A	900	120,000	$P_{RD} = 8.78 \times 10^{-5}$		
1	270	119,500	.16[1]	1.24	.85
2	180	119,000	3.08	2.75	.89
3	240	118,000	5.40	4.84	.90
4	250	117,500	8.10	7.29	.90
5	160	117,000	13.2	12.4	.94
6	150	116,000	17.8	16.7	.94
7	140	113,000	26.0	24.2	.93
8	90	106,000	71.0	65.5	.92
9	100	103,000	94.0	92.8	.99
B	550	99,500	$P_{RD} = 1.02 \times 10^{-4}$		

TABLE 3

Experimental Data for He on Fresh Silver - July 23

Run No.	Time Sec.	Approx. RPM	P_G Torr x 10^{-4}	$(P_S)_{cor}$ Torr x 10^{-4}	σ
A	900	131,000	$P_{RD} = 2.57 \times 10^{-4}$		
1	290	130,000	3.74	.77	.21
2	210	129,500	8.10	2.30	.28
3	280	129,400	12.2	4.62	.38
4	240	129,200	20.9	8.21	.39
5	320	129,000	21.8	8.42	.38
6	420	128,200	34.2	14.0	.41
7	390	128,200	35.2	14.5	.41
8	260	123,400	149.	72.6	.49
9	240	120,000	230.	109.	.47
B	1050	117,000	$P_{RD} = 2.77 \times 10^{-4}$		

TABLE 3a

Repeat - He on Fresh Silver - July 24

Run No.	Time Sec.	Approx. RPM	P_G Torr x 10^{-4}	$(P_S)_{cor}$ Torr x 10^{-4}	σ
A	1000	147,500	$P_{RD} = 2.53 \times 10^{-4}$		
1	280	147,000	1.45	6.05	.42
2	320	146,000	35.5	17.8	.50
3	250	145,000	52.2	27.9	.53
4	290	143,000	123.	42.7	.35
5	180	138,000	152.	105.	.69
B	690	135,000	$P_{RD} = 2.69 \times 10^{-4}$		

TABLE 4

Experimental Data for A on Fresh Silver - July 24

Run No.	Time Sec.	Approx. RPM	P_G Torr x 10^{-4}	$(P_S)_{cor}$ Torr x 10^{-4}	σ
A	700	135,000	$P_{RD} = 8.59 \times 10^{-5}$		
1	330	134,500	2.51	2.22	.88
2	430	133,000	4.70	4.57	.94
3	330	132,000	6.50	6.32	.97
4	340	131,000	9.76	9.80	1.00
5	300	129,000	12.3	12.2	.99
6	100	127,000	12.9	22.8	Valve
B	460	113,800	$P_{RD} = 9.72 \times 10^{-5}$		Leaking

TABLE 5

Experimental Data for N_2 on Aged Silver - July 26

Run No.	Time Sec.	Approx. RPM	P_G Torr x 10^{-4}	$(P_S)_{cor}$ Torr x 10^{-4}	σ
A	1050	152,000	$P_{RD} = 2.23 \times 10^{-4}$		
1	210	150,500	1.40[1]	1.22	.87
2	280	150,200	2.50[1]	2.39	.95
3	350	150,000	3.80	3.57	.94
4	280	149,500	5.70	5.29	.93
5	250	146,200	8.50	7.82	.92
6	350	146,000	11.2	10.2	.92
7	240	145,000	13.7	13.1	.96
8	250	143,000	17.2	16.7	.97
9	150	141,500	18.0	17.2	.95
10	170	140,000	30.5	27.8	.92
11	100	138,000	38.5	35.3	.92
12	100	136,000	65.0	60.3	.93
13	110	132,000	95.0	89.5	.94
14	170	128,000	132.	124.	.94
B	820	120,000	$P_{RD} = 2.55 \times 10^{-4}$		
C	170	147,200	$P_{RD} = 2.32 \times 10^{-4}$		
15	220	147,000	.92[1]	.89	.91
16	190	146,700	1.65[1]	1.60	1.00
17	210	146,500	2.85	2.62	.92
18	170	146,000	4.20	3.82	.91
19	210	145,500	8.45	7.63	.90
20	200	144,500	12.8	12.1	.95
21	170	143,500	21.5	20.3	.95
22	130	141,500	32.5	30.3	.93
23	160	139,500	52.6	47.8	.91
24	180	136,000	77.0	70.5	.92
25	130	130,000	115.	107.	.93
D	700	125,000	$P_{RD} = 2.50 \times 10^{-4}$		

TABLE 6

Experimental Data for He on Aged Silver - July 27

Run No.	Time Sec.	Approx. RPM	P_G Torr x 10^{-4}	$(P_S)_{cor}$ Torr x 10^{-4}	σ
A	550	124,500	$P_{RD} = 2.56 \times 10^{-4}$		
1	170	121,000	8.34[1]	6.56	.79
2	250	121,500	13.1[1]	11.0	.84
3	180	120,500	20.9	18.2	.87
4	180	120,000	28.5	23.2	.82
5	180	119,000	36.1	32.5	.90
6	180	118,000	47.6	43.5	.92
7	150	117,000	76.0	70.0	.92
8	200	115,000	97.8	92.0	.94
9	170	112,500	100.[1]	102.	1.00
10	150	109,500	171.[1]	162	.95
B	2000	107,000	$P_{RD} = 2.52 \times 10^{-4}$		

TABLE 7

Experimental Data for A on Aged Silver - July 27

Run No.	Time Sec.	Approx. RPM	P_G Torr x 10^{-4}	$(P_S)_{cor}$ Torr x 10^{-4}	σ
A	540	137,250	$P_{RD} = 8.05 \times 10^{-5}$		
1	270	137,000	.98[1]	.11	.12
2	190	136,750	1.55[1]	1.40	.90
3	220	136,500	3.57	3.15	.88
4	250	136,000	5.43	4.99	.92
5	230	135,000	8.00	7.50	.94
6	220	134,500	11.7	9.90	.85
7	230	133,500	14.2	13.7	.96
8	160	131,500	21.4	19.7	.92
9	180	129,000	32.8	29.6	.91
10	150	126,500	50.0	46.0	.92
11	120	122,000	71.4	64.6	.91
12	160	118,000	96.0[1]	78.2	.81
B	590	99,250	$P_{RD} = 8.65 \times 10^{-5}$		